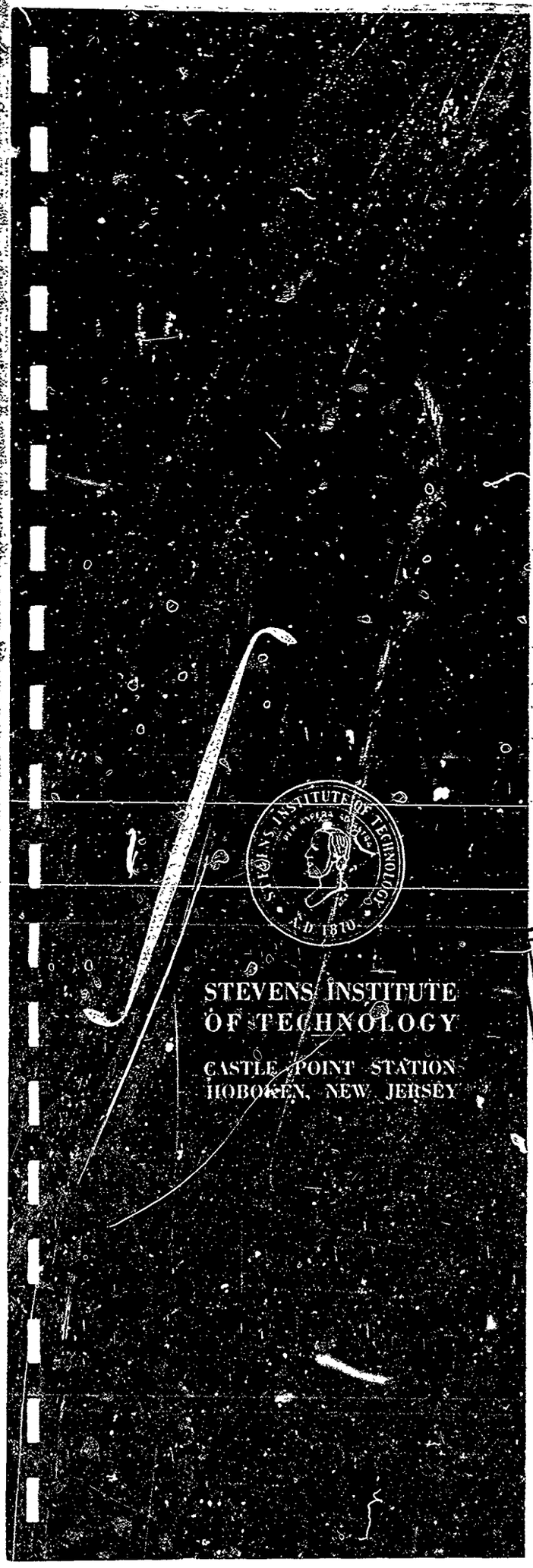

DAVIDSON LABORATORY

Report SIT-DL-71-1554

September 1971

NORMAL AND SHEAR STRESS DISTRIBUTION UNDER A RIGID WHEEL IN DRY SAND

by

Samuel E. Shamay

prepared for

Department of Defense
under
Contract DAAE-07-69-0356

(Project Themis)

UNCLASSIFIED
Security Classification

DOCUMENT CONTROL DATA - R & D

Security classification of title, body of abstract and indexing annotation must be entered when the overall report is classified)

1 ORIGINATING ACTIVITY (Corporate author) Davidson Laboratory, Stevens Institute of Technology Hoboken. New Jersey 07030	2a. REPORT SECURITY CLASSIFICATION UNCLASSIFIED 2b. GROUP

3 REPORT TITLE

NORMAL AND SHEAR STRESS DISTRIBUTION UNDER A RIGID WHEEL IN DRY SAND

4 DESCRIPTIVE NOTES (Type of report and inclusive dates)

Final Report

5 AUTHOR(S) (First name, middle initial, last name)

Samuel E. Shamay

6 REPORT DATE	7a. TOTAL NO. OF PAGES	7b. NO. OF REFS
September 1971	87	16

8a. CONTRACT OR GRANT NO.	9a. ORIGINATOR'S REPORT NUMBER(S)
DAAE-07-69-0356 b. PROJECT NO.	
c.	9b. OTHER REPORT NO(S) (Any other numbers that may be assigned this report)
d.	

10 DISTRIBUTION STATEMENT This document has been approved for public release and sale; its distribution is unlimited. [redacted] of the document in whole or in part is permitted for any purpose of the U.S. Government.

11. SUPPLEMENTARY NOTES	12. SPONSORING MILITARY ACTIVITY
	Department of Defense Washington, D. C. 20301

13. ABSTRACT

A very sensitive transducer was developed in order to measure the normal pressure and the shear stresses simultaneously on the rim of a rigid wheel moving in fine sand.

Four of these transducers were installed across the wheel width to measure the lateral stress distribution as well.

A series of tests were conducted for a driven wheel on soft sand. The tests were performed at both positive and negative slip rates. For each slip rate, the wheel load, the wheel sinkage, the torque due to the soil on the wheel rim, and the stress distribution in the soil were measured and recorded.

In order to validate the results, the recorded stresses were integrated to yield the forces and moments acting on the wheel-soil interface. These forces and moments were then compared to the actual measured forces and torque.

The measured stress distribution was compared to calculated stresses using Bekker's and Sela's equations for pressure sinkage relationships. Sela's equations yield better correlation than did those by Bekker, although both are restricted to the zero slip condition.

For non-zero slip conditions the actual stress distribution was compared to the zero slip stresses in order to find the deviation due to slip.

14 KEY WORDS	LINK A		LINK B		LINK C	
	ROLE	WT	ROLE	WT	ROLE	WT
PRESSURE DISTRIBUTION						
SHEAR STRESSES						
SOIL-VEHICLE MECHANICS						
TRANSDUCERS						

DAVIDSON LABORATORY
Stevens Institute of Technology
Castle Point Station
Hoboken, New Jersey 07030

Report SIT-DL-71-1554

September 1971

NORMAL AND SHEAR STRESS DISTRIBUTION UNDER A RIGID WHEEL IN DRY SAND

by

Samuel E. Shamay

Prepared for
Department of Defense
under
Contract DAAE-07-69-0356
(DL Project (3683/423)

Approved

I. Robert Ehrlich, Manager
Transportation Research Group

ABSTRACT

NORMAL AND SHEAR STRESS DISTRIBUTION

UNDER A RIGID WHEEL IN DRY SAND

by

Samuel E. Shamay

Advisor

Dr. I. R. Ehrlich

May 1971

A very sensitive transducer was developed in order to measure the normal pressure and the shear stresses simultaneously on the rim of a rigid wheel moving in fine sand.

Four of these transducers were installed across the wheel width to measure the lateral stress distribution as well.

A series of tests were conducted for a driven wheel on soft sand. The tests were performed at both positive and negative slip rates. For each slip rate, the wheel load, the wheel sinkage, the torque due to the soil on the wheel rim, and the stress distribution in the soil were measured and recorded.

In order to validate the results, the recorded stresses were integrated to yield the forces and moments acting on the wheel-soil interface. These forces and moments were then compared to the actual measured forces and torque.

The measured stress distribution was compared to calculated stresses using Bekker's and Sela's equations for pressure sinkage relationships. Sela's equations yield better correlation than did those by Bekker, although both are restricted to the zero slip condition.

For non-zero slip conditions, the actual stress distribution was compared to the zero slip stresses in order to find the deviation due to slip.

KEYWORDS

Pressure Distribution

Shear Stresses

Soil-Vehicle Mechanics

Transducers

TABLE OF CONTENTS

Table of Contents
(continued)

LIST OF SYMBOLS

A	Area	in^2
b	Wheel Width	in
c	Soil Coefficient of Cohesion	lb/in^2
D	Wheel Diameter	in
DP	Drawbar Pull Force	lb
h	Soil Plate Edge Effect Coefficient	lb/in
i	Slip Rate	dimensionless
j	Soil Deformation	in
k	Bernstein's Modulus of Soil Deformation	lb/in^{n+2}
k_c	Cohesive Modulus of Soil Deformation	lb/in^{n+1}
k'_c	Sela's Cohesive Modulus of Soil Deformation	lb/in^{n+1}
k_φ	Frictional Modulus of Soil Deformation	lb/in^{n+2}
K	Slip Coefficient	in
M	Number of Carriage Microswitch Contacts	dimensionless
n	Exponent of Soil Deformation	dimensionless
N	Normal Force	lb
N_h	Horizontal Component of Normal Force	lb
N_v	Vertical Component of Normal Force	lb
p	Soil Pressure	lb/in^2
P_i	Initial Soil Pressure	lb/in^2
Q	Wheel Input Torque	ft-lb
R_h	Hydraulic Radius	in
s	Tangential Stress	lb/in^2

List of Symbols
(continued)

t_c	Time for a Segment of Test Run	sec
t_w	Time Required to Complete One Wheel Revolution	sec
T	Tangential Shear Force	ft-lb
T_h	Horizontal Component of T	lb
T_v	Vertical Component of T	lb
V_c	Carriage Velocity	ft/sec
V_w	Wheel Velocity	ft/sec
W	Total Wheel Load	lb
z	Wheel Sinkage	in
z_i	Imaginary Sinkage	in

Greek Letters

α	Angle of Action of Normal Force	deg
α_1	Angle of Entry	deg
α_2	Angle of Exit	deg
φ	Soil Angle of Internal Friction	deg

LIST OF FIGURES

List of Figures
(continued)

List of Figures
(continued)

LIST OF TABLES

1. BACKGROUND

1-1 Historical Background

It is traditional to trace the development of vehicle-soil mechanics over some two hundred years. However, the foundation of present theoretical work is the efforts of the British Army and Bekker[1] and his colleagues in the U.S.A. Micklethwaite[2] was the first to apply the principles of civil engineering soil mechanics to the vehicle problem. More recent work by Evans[3] and Uffelman[4] was confined to frictionless clays. An attempt to develop a theory applicable to all soils was made by Bekker[5]. Although yielding first-order results, for practical purposes, this theory lacks precision.

Most recently a study by Sela and Ehrlich[6,7] presented a significant improvement upon Bekker's method of predicting the performance of wheels, tracks, and other vehicle tractive elements. In order to obtain a better understanding of the problems involved, it is desirable to compare the actual stress distribution beneath a wheel with that predicted by Sela and Ehrlich.

Earlier workers in this field measured the normal stress field under wheels by means of various transducers embedded in the soil. Vincent[8] and Hegedus[9] used small wheels and measured only the radial stresses using diaphragm type pressure cells. These methods suffer from the disadvantage that tangential stresses are neglected and did not ascertain the pressure distribution across the width of the rim. Uffelman[4] attempted to measure the tangential stresses using a sensing strip, but he measured the radial and tangential stresses on two

different points on the wheel rim, which caused considerable difficulties in correlating the data measured. Sela[10] used a single element at the center of the wheel width. Onafeko and Reece[11] measured radial and shear stresses by a single element which spanned the entire width of the wheel. Most recently Krick[12] measured the stress distribution in three directions (lateral, radial and tangential) to give a better insight of the problem.

1-2 General Theory

A rigid wheel rolling on soft soil sinks into it and causes strains and stresses in the soil. These stresses cause the reactions which balance the system of forces imposed on the wheel (load, drawbar-pull, torque, etc.).

Assuming a uniform stress distribution, we resolve the stresses into normal and tangential components. The normal stresses act perpendicular to the wheel axis. Thus the differential normal force, dN , (Figure 1) is given by:

$$dN = pb\frac{D}{2}\,d\alpha$$

where:

p = pressure

b = wheel width

N = normal force

α = angle of action of normal force

D = wheel diameter

This force can be resolved into a horizontal and vertical component which contribute in balancing the drawbar-pull DP and load W on the wheel, respectively.

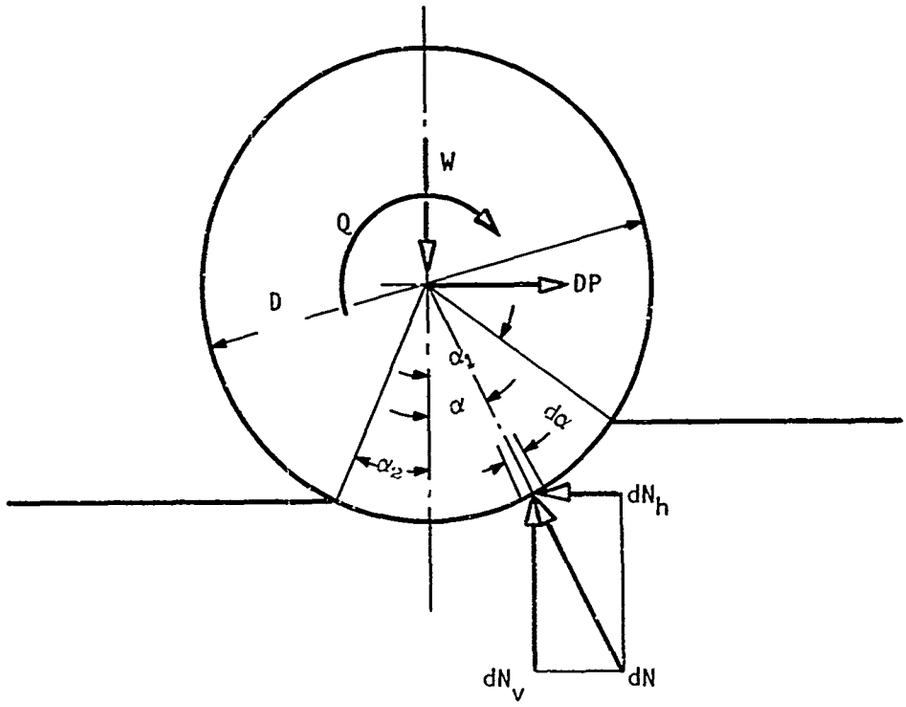

FIG. 1. NORMAL STRESS ANALYSIS

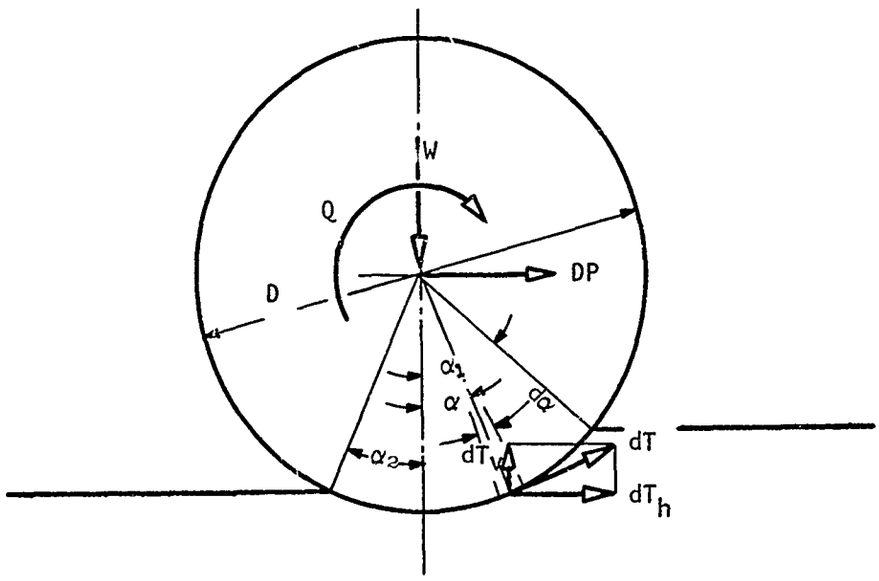

FIG. 2. TANGENTIAL STRESS ANALYSIS

Therefore:

$$dN_h = dN \sin\alpha = pb\frac{D}{2} \sin\alpha \, d\alpha$$

and

$$dN_v = dN \cos\alpha = pb\frac{D}{2} \cos\alpha \, d\alpha$$

The shear stresses act tangentially to the wheel circumference. Thus the differential tangent force dT (Figure 2) is given by:

$$dT = \frac{D}{2} s \, b \, d\alpha$$

where:

T = tangential force

s = shear stress

This force can be resolved into a horizontal and vertical component, which contribute to balance the drawbar-pull, DP, and the weight and load, W:

$$dT_h = dT \cos\alpha = sb\frac{D}{2} \cos\alpha \, d\alpha$$

$$dT_v = dT \sin\alpha = sb\frac{D}{2} \sin\alpha \, d\alpha$$

N is radially directed so it does not contribute to balance the input torque Q. The only force which balances the input torque Q, is due to the shear stresses:

$$dQ = sb\left(\frac{D}{2}\right)^2 d\alpha$$

Accordingly, the system of forces acting on the wheel, mainly load, W, drawbar-pull, DP, and torque, Q, is balanced by the sum of the various components of the stresses.

$$W = N_v + T_v = \int_{\alpha_2}^{\alpha_1} dN_v + \int_{\alpha_2}^{\alpha_1} dT_v$$

$$= b\frac{D}{2}\int_{\alpha_2}^{\alpha_1} p(\alpha)\cos\alpha\, d\alpha + b\frac{D}{2}\int_{\alpha_2}^{\alpha_1} s(\alpha)\sin\alpha\, d\alpha \qquad (1)$$

$$DP = -N_h + T_h = -\int_{\alpha_2}^{\alpha_1} dN_h + \int_{\alpha_2}^{\alpha_1} dT_h$$

$$= -b\frac{D}{2}\int_{\alpha_2}^{\alpha_1} p(\alpha)\sin\alpha\, d\alpha + b\frac{D}{2}\int_{\alpha_2}^{\alpha_1} s(\alpha)\cos\alpha\, d\alpha \qquad (2)$$

$$Q = b\left(\frac{D}{2}\right)^2 \int_{\alpha_2}^{\alpha_1} s(\alpha)\, d\alpha \qquad (3)$$

NOTE: In the integrations above, we assume a uniform stress distribution across the wheel width. The experiments show that this is not true but that the lateral distribution is linear. Then taking an average value for p and s we can perform the integrations.

2. TECHNICAL DISCUSSION

2-1 The Normal Stresses

Equations (1,2,3) are always valid because they are developed from equilibrium considerations. However, their utility for predicting wheel performance is very limited, due to the fact that actual stress measurements are needed in order to use them.

Equation (4), describing the pressure as a function of wheel sinkage and soil properties, was developed by Bekker[1] based on experiments with flat plates:

$$p = \left(k_\varphi + \frac{k_c}{b}\right) z^n = kz^n \qquad (4)$$

where:

- p - pressure on a flat plate
- z - depth of plate penetration
- n - a soil property
- b - the plate width
- k_m, k_φ - parameters of the soil
- $k = k_\varphi + \frac{k_c}{b}$

Equation (4) has often been criticized on the ground that it is in contradiction with well established bearing capacity theories and the dimensions of k_c , k_φ are a function of n.

In order to overcome these disadvantages, Reece[13] proposed:

$$p = \left(ck_c' + \gamma b\, k_\varphi'\right) (z/b)^n$$

where c, k'_c, k'_φ, n are true soil parameters independent on plate size.

Reece's equation did not yield better results than Bekker's because they had common shortcomings as stated by Sela:[6]

> "They predicted well only in the sinkage range, and for the plate sizes and shapes near that of the experimental tests; they are not able to predict well the performance of plates of greatly different sizes; and they cannot predict the performance of plates of different shape."

To overcome these shortcomings, Sela and Ehrlich[6] recently developed an improved equation for flat plates:

$$p = p_i + \frac{h}{R_h} + \left(k_\varphi + \frac{k'_c}{R_h}\right)(z_i + z)^n \qquad (5)$$

where:

- p - the nominal soil pressure under a plate
- p_i - the initial soil bearing capacity, independent of plate shape (a parameter of the soil)
- h - the initial soil bearing capacity, dependent on plate shape (a parameter of the soil)
- R_h - hydraulic radius of the plate $\frac{\text{plate area}}{\text{plate perimeter}}$
- k_φ - the soil strength modulus, independent of plate shape
- k'_c - the soil strength modulus, dependent on plate shape
- z_i - the degree of compaction, dependent on previous loads on the soil (a parameter of the soil)
- z - the sinkage into the soil, at which the nominal pressure p, is measured
- n - the soil sinkage exponent (a parameter of the soil)

If, in Equation (5) we let:

$$p_o = p_i + \frac{h}{R_h}$$

and

$$k = k_\varphi + \frac{k'_c}{R_h}$$

We now have:

$$p = p_o + k(z_i + z)^n \tag{6}$$

Experiments indicate that p_o tends to be zero in frictional soils; therefore, for sand, which is purely frictional,

$$p = k(z_i + z)^n \tag{7}$$

2-2 The Shear Stresses

The shear stress distribution, is a much more complex problem, because it is a function of wheel slip. Many theories have been developed to understand and solve the problem, but up to now, none have been able to predict accurately the shear stress distribution under a rigid wheel rolling in sand. The following is a brief summary of these works.

Bekker[1] proposed a general equation to describe all the possible forms of the experimental shear stress-deformation curve. He did this empirically by adapting an equation relating the displacement and natural frequency of a periodic vibration which gave the desired form of the curve.

$$s = (c + p\tan\varphi)\left[\frac{e^{(-k_2 + \sqrt{k_2^2 - 1})k_1 j}}{Y_{max}} - \frac{e^{(-k_2 - \sqrt{k_2^2 - 1})k_1 j}}{Y_{max}}\right] \quad (8)$$

where:

k_1, k_2 are soil deformation constants

Y_{max} is the maximum value of the exponential obtained by substituting j_{max}

j_{max} the deformation for maximum shear

Measurements and calculation of k_1, k_2 are very tedious and inaccurate. Sela[14] developed a more precise but somewhat complicated way of measuring these values.

A much simpler experimental equation was proposed by Janosi[15] which only involved the two strength parameters and one deformation constant K. The soil shear stress is given by:

$$s = (c + p\tan\varphi)(1 - e^{-\frac{j}{k}}) \quad (9)$$

Equation (9), much easier to manipulate, is today widely used in place of Equation (8). In fact it has been the base of almost all other investigations of this subject. These investigations were mainly directed at finding an equation describing the deformation of the soil under stress. Janosi[15] was the first to present an equation based on the wheel kinematics. He derived an equation for the path of a particle on the wheel rim, which is a looped cycloid. It has the form:

$$j = \frac{D}{2}\left[(1 - i_o)(\theta_o - \theta) + \sin\theta - \sin\theta_o\right]$$

where:

θ_o is the angle of contact of the wheel soil interface

θ is the angle from the vertical, and

i_o is the wheel slip.

This equation varies for different portions of the contact angle. Substituting j in Equation (9) one obtains the shear distribution and the normal to shear stress relationship. Janosi himself recognizes that this method involves a number of gross approximations and crude assumptions.

Reece and Onafeko[11] criticizing Janosi's approach to the problem wrote:

"There are three things basically wrong with Janosi's theory:

a) The analysis starts by resolving the total stress on an element of the rim into radial and tangential components. There is no justification for further resolving one of these components into vertical and horizontal components. There are no grounds for distinguishing between the horizontal component of the radial and tangential stresses.

b) In the basic shear deformation test, the shear stress is related to a deformation in the same direction. Janosi assumes that the same numerical relationship will apply when the stress is at an angle to the deformation. This angle can be as large as 60^o in practice.

c) There is no justification for the choice of the horizontal soil deformation as the one which gives rise to the shear stresses, which are in a different direction."

Uffelman[4] working on non-frictional soils assumed a uniform tangential force distribution and showed that for purely cohesive soils, a cylindrical wheel with no side walls would fail at a fixed sinkage irrespective of actual value of soil cohesion or wheel width. Experiments validate his theory but it is limited only to purely cohesive soils.

Vincent[8] investigated the flow of sand past a rigid wheel and recorded normal pressure distribution under the wheel in dry sand. He concluded that for a towed wheel:

"a) Compaction effects are small

b) Flow of sand occurs as a result of bulldozing forming a bow wave.

c) The normal pressure of the sand against the surface of the wheel is of the form $p = kz^n$.

d) The pressure of the sand on the surface of a wheel can best be represented by two sets of soil values, one during compaction and the other as the stress is relieved.

e) He acknowledges that flow, as the main process for the conditions considered, offers a more realistic approach to the problem."

Hegedus[9] continued Vincent efforts by measuring the normal pressure distribution under rigid wheels. Summarizing his test results he wrote:

"a) The driving torque which depends on the tangential forces becomes constant in sand when slip exceeds 30%. Thus the assumption that φ = constant along the wheel soil interface is valid at least above 30% slip.

b) The sinkage and the shape of the normal pressure distribution depend on slip.

c) The pressure is not zero at $\theta = 2\pi$.

d) Lateral pressure distribution is not constant."

Sela[10] working on dry sand which is purely frictional, used Equation (9) where $c = 0$:

$$s = p\tan\varphi\left(1 - e^{-\frac{j}{k}}\right)$$

In calculating j, Sela introduced the simple assumption that:

$$j = \frac{D}{2}(\alpha - \alpha_o)i_o$$

where:

α_o = contact angle

α = angle from the vertical

thus assuming that the wheel behaves like a track. That is, the deformation is in the direction of the stress and varies proportionally to its distance from the leading edge. However, he introduced a coefficient of proportionality, m, the behaviour of which he did

not establish, thus leaving the problem open, although "a better understanding of the skidding wheel-soil relationship was established."

Onafeko, Wong and Reece[11] re-evaluating the kinematics of the wheel and the path of the particles on its rim derived an expression for j:

$$j = \frac{D}{2}\left[(\theta_1 - \theta) - (1 - i)(\sin\theta_1 - \sin\theta)\right] \qquad (10)$$

where:

θ_1 is the entry angle, that is, the coordinate of the point where rim and soil surface meet

Although strictly correct mathematically, Equation (10) did not check satisfactorily with experiments. Criticizing this approach Weindieck[16] stated that no true relationship could be correct taking into consideration only the wheel kinematics. The complex soil flow should be included as well.

Following Reece, many investigators tried to relate the shear stresses and the tractive effort using energy considerations as an approach. Others used the more sophisticated techniques of photoelasticity to determine the flow of soil under rigid wheels. However, no satisfactory equation, predicting tractive effort performance accurately, is known today.

The last one known to have measured stress distribution under rigid wheels in sand is Krick[12]. However, he did not develop prediction equations.

3. TEST OBJECTIVES

In view of the above, accurate measurements were needed to understand the wheel sinkage phenomena and to analyze it. Actually, there were two major objectives to this series of tests: first, to compare measured and predicted pressure distributions under a rigid wheel for the no-slip condition, secondly, to generate measured data for non zero slip for use in future studies.

A third objective, which was no small task, was to make the new wheel dynamometer operational. At the start of this program, the dynamometer had just been delivered from the manufacturer. It was necessary, before the program could commence, to check out, modify, and calibrate the entire system. Actually, this part consumed more than 80% of the time used in this work.

4. DESCRIPTION OF APPARATUS AND TEST PROCEDURES

4-1 Soil Bin

The tests were performed in the Davidson Laboratory soil bin dynamometer. It is 37 feet long, 3 feet wide and filled to a depth of 24 inches with fine grain sand. The angle of internal friction φ was measured to be 31^{o}. The sand was air dry and contained a moisture content which varied between 0.6% and 1.0% by weight. Using the flat plate bevameter technique the soil sinkage parameters were determined to be:

$k_{\varphi} = 4.7 \text{ lb/in}^{n-2}$

$k_c = 0$

$n = 1.15$

soil cohesion was negligible

Sela's soil parameters, which are used in this study were computed to be:

$p_o = 0$

$z_i = 0.85$ inches

$n = 1.51$

$k_{\varphi} = 2.7 \text{ lb/in}^{n-2}$

$k'_c = -0.5$

The soil was processed with a gyrotiller and levelling plate before each test (see Fig. 3). The depth of the tillage was 18 inches and the levelling plate insured a sand surface which was parallel to the carriage rails. The sand was tilled sufficiently during the

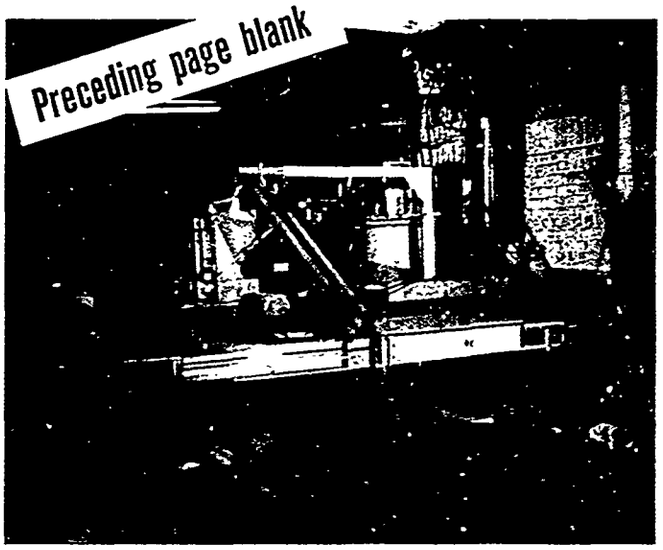

FIG. 3. SOIL PROCESSING UNIT

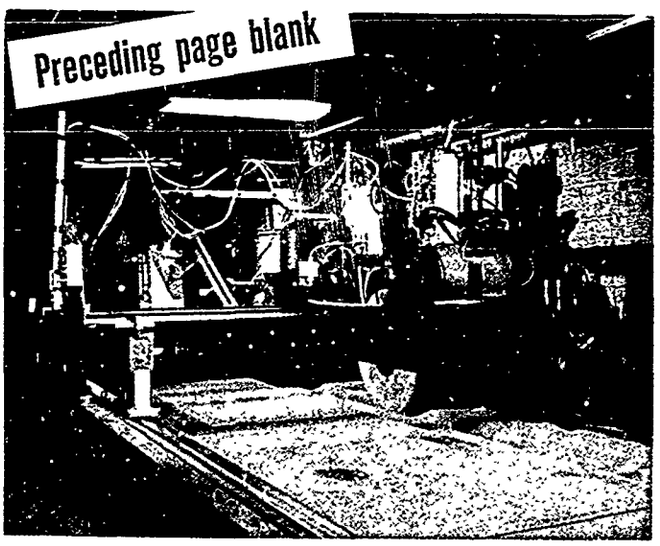

FIG. 4. WHEEL DYNAMOMETER

test period to maintain it in a uniformly air-dry condition.

After processing the soil, penetration readings (standard WES cone penetrometer) and shear strength readings (Cohron shear graph) were taken at $1\frac{1}{2}$ foot intervals along the centerline of the wheel path to assure that soil properties did not vary significantly during the test program.

4-2 Wheel Dynamometer

For the purpose of the project, of which this study is a part, a new wheel dynamometer was built (see Figure 4). By means of extremely sensitive gauges mounted on the wheel shaft, this dynamometer is able to measure all six orthogonal forces and moments acting on the wheel.

The wheel shaft is mounted on a construction which is able to move up and down as well as sideways and is driven by a hydraulic system.

This construction itself is mounted on a carriage moving on rails above the soil bin by means of an electric motor and a chain-sprocket arrangement. Thus the wheel can be easily moved in any desired direction.

The wheel shaft is rotated by a hydraulic motor allowing an infinite variation of speed.

The vertical load applied on the wheel is obtained by means of a pneumatic system. By adjusting a difference of pressure between two reservoirs, the load on the wheel remains constant regardless of wheel sinkage. A similar system enables one to maintain a constant

horizontal force sideways; however, this system was not used for these tests.

The wheel motor is driven by a hydraulic pump which, in turn, is driven by an electric motor mounted on the carriage. All the controls are electronic.

4-3 Instrumentation

a. General

The following quantities were measured and recorded:

W	Vertical load on the wheel	lbs
DP	Drawbar-pull	lbs
T	Torque	ft/lbs
z	Wheel sinkage	inches
V_w	Wheel velocity	ft/sec
V_c	Carriage velocity	ft/sec
α	Position of the transducers (Angle from B.D.C.)	degrees
N	Normal forces	lbs
T	Shear forces	lbs

The vertical load on the wheel was measured by a very sensitive semiconductor strain gauge mounted on the wheel shaft. This gauge was calibrated using dead weight loads.

In a similar way, gauges of the same kind, mounted on different locations on the wheel shaft, were used to measure the drawbar-pull force and the torque applied on the wheel.

During calibration all interactions between gauges were measured to enable corrections for cross-talk of the recorded data.

The wheel sinkage was measured with a rotary potentiometer mounted on the dynamometer carriage and referenced from the soil surface. The wheel speed was controlled by adjusting a valve on the hydraulic motor. These revolutions were measured by means of a microswitch which opened when it contacted small screws specially mounted on the wheel side well.

The carriage velocity was varied by changing the speed of the electric drive motor. The carriage velocity was measured through a microswitch which contacted event markers located at one foot intervals along the side rail of the soil bin.

The position of the transducers was measured by the angle their radial axis made with the bottom-dead-center of the wheel. This was achieved by means of a microswitch activated by event markers mounted on the wheel side 5^{o} apart.

b. Transducers Design

To measure the normal and shear stresses, a special transducer was designed. The basic requirements in the design were:

a) Measurement of forces in horizontal and vertical direction simultaneously.

b) As little as possible force interaction readings.

c) Transducer outputs should not be affected by the position of the line of action of the forces.

d) Transducers should be small and as sensitive as possible.

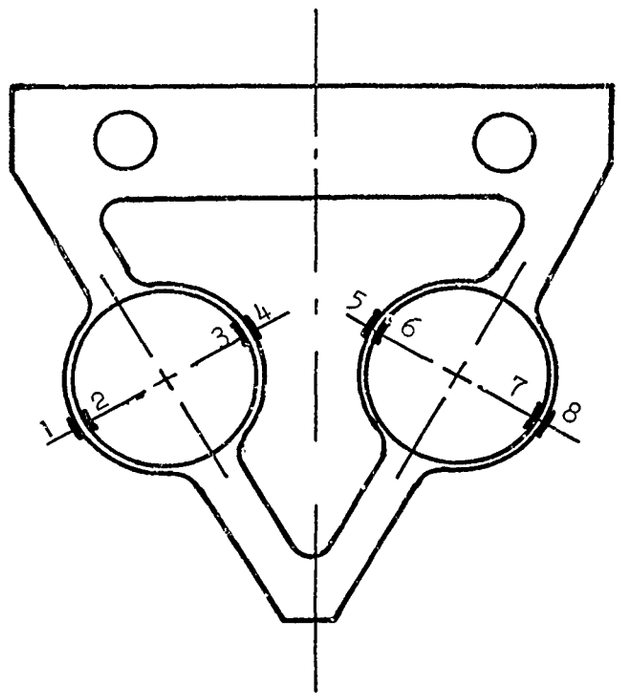

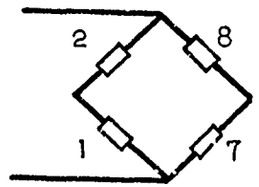

Normal

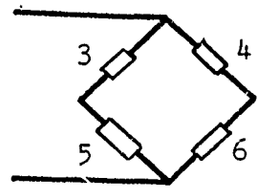

Tangential

FIGURE 5. EARLY TRANSDUCER DESIGN AND WIRING

First the investigations were directed at ring-like transducers, which could achieve all the requirements above, using standard wire strain gauges. They were designed so that by mounting the gauges on the side of the rings and adding them in a wheatstone bridge, we could get four times the output of one gauge (see Figure 5).

This design was abandonned when we found out that we could use semi-conductor gauges with 10-20 times larger outputs. Using these gauges, we then turned to cantilever beams configurations. The final design of the transducer consists of an L-shaped cantilever beam on which semi-conductor gauges are cemented (see Figures 6 and 7). Due to the extreme sensitivity of the gauges, we could still have large enough readings after subtracting the outputs of gauges on the same arm of the transducer. This subtraction achieved by putting the two outputs of the gauges in adjacent arms of a wheatstone bridge enables us to cancel the influence of other forces on this arm, since they produce the same constant moment (see Figure 8).

For calibration purposes, a special rig was built (Figure 9) with which dead weights were used. Calibration showed that the gauges gave linear outputs. Shear forces influenced the normal outputs by 5% at the most, while normal forces did not have any readable influence on the shear gauges readings. Due to the exact location of the gauges, lateral forces did not have any influence on either the normal or the shear forces gauges.

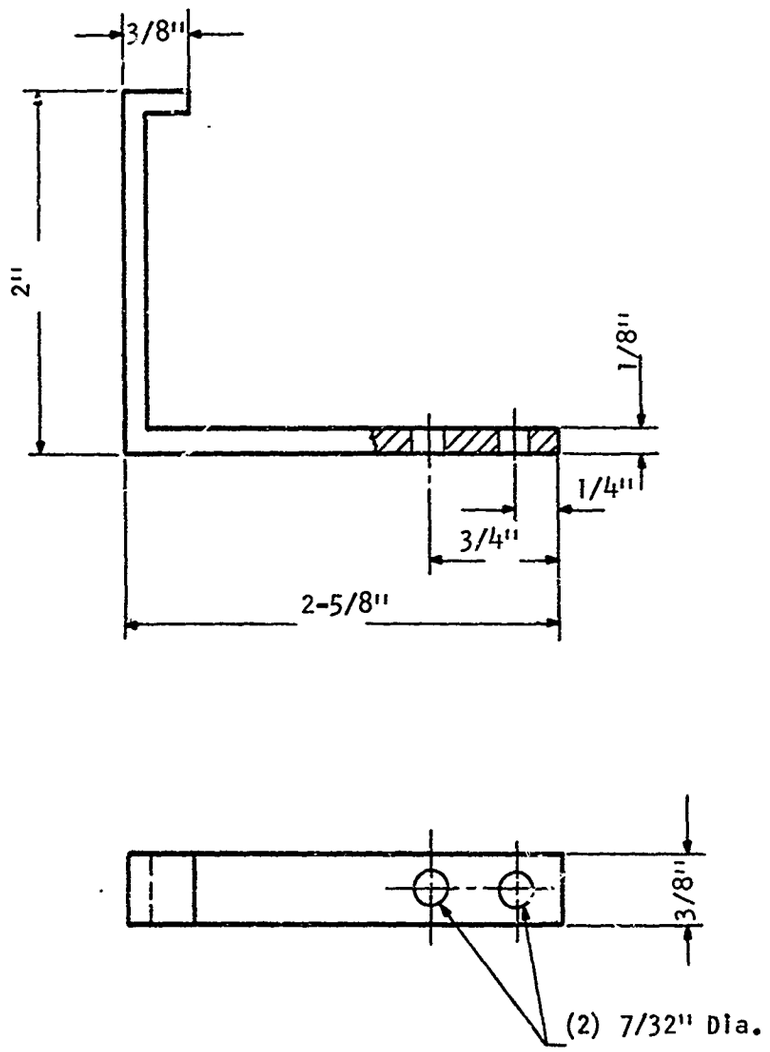

FIG. 6. TRANSDUCER DESIGN

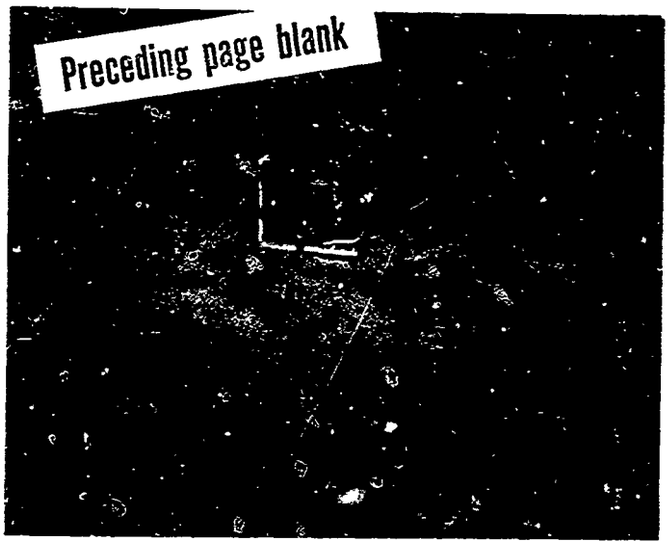

FIG. 7. TRANSDUCER WIRING

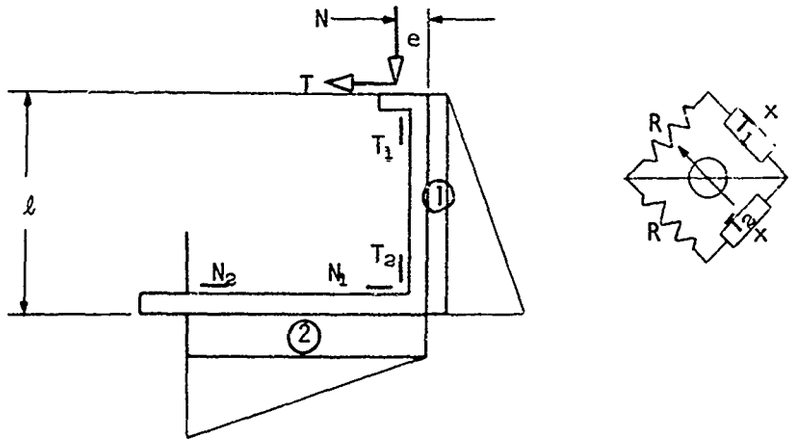

① Constant moment due to N x e

② Constant moment due to T x ℓ and N x e

By substracting the outputs of T_1, T_2 and N_1, N_2, we record only the varying moments. The vertical arm measures the tangential stresses only while the horizontal arm measures the normal stress.

FIG. 8. TRANSDUCER WORKING PRINCIPLE

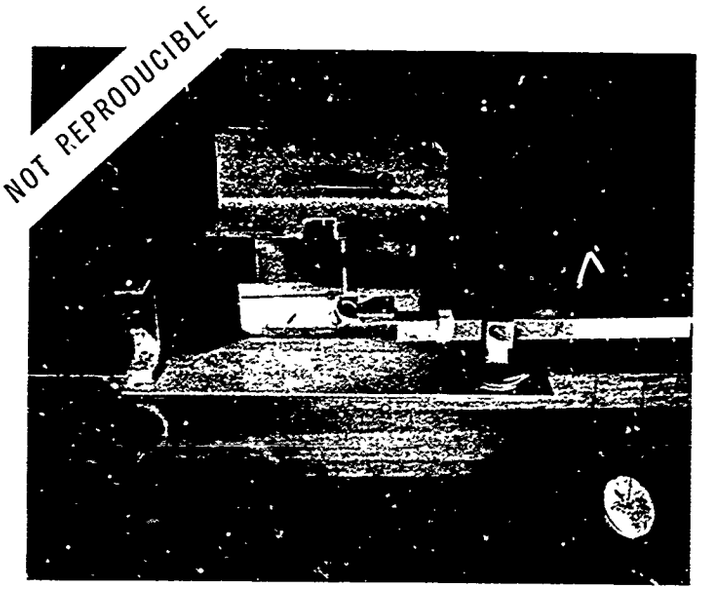

FIG. 9. CALIBRATION RIG FOR TRANSDUCER

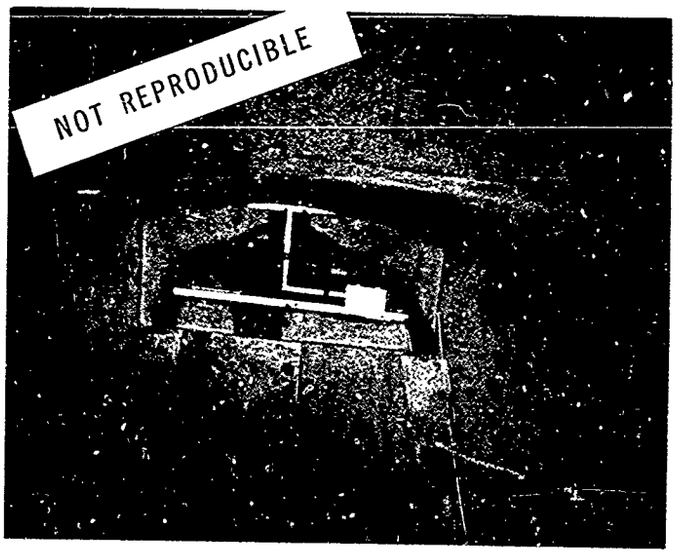

FIG. 10. TRANSDUCERS INSTALLED IN WHEEL
SIDE VIEW

c. Wheel Construction and Transducer Installation

The wheel was made of individual sheets of marine grade plywood. Each sheet was initially cut slightly oversize and then aligned and bolted together into the desired thickness of the wheel. The assembled wheel was then cut to final size on a band saw fitted with a circle cutting attachment. Then the wheel was carved out to accommodate the transducers (see Figure 10). The soil being quite homogeneous and no side forces being applied, the pressure and shear stress distributions are symmetrical. The transducers were inserted into only half of the wheel width (Figure 11). Four transducers were mounted to a carrying plate. They were numbered so that transducer no. 1 was installed in the middle of the wheel and others covered the surface up to one-eighth inch from the edge of the wheel.

The carrying plate was installed into the cut-out on the wheel. The side opening in the wheel was covered with an aluminum plate fitted so that it was flush with the wheel. On the circumference, a plate with windows fitted to the transducers was shaped and adjusted so that it would not change the wheel profile. In order to be sure that the slip occurred between layers of sand and not between the sand-wheel interface (Figures 11 and 12). The wheel rim, as well as the measuring surfaces were covered with coarse sand paper.

One of the major problems was the sealing of the gaps between the wheel and the transducers. Many techniques were tried but, the transducer being very sensitive, picked up inputs due to the sealing forces. The idea of sealing the gaps was to protect the

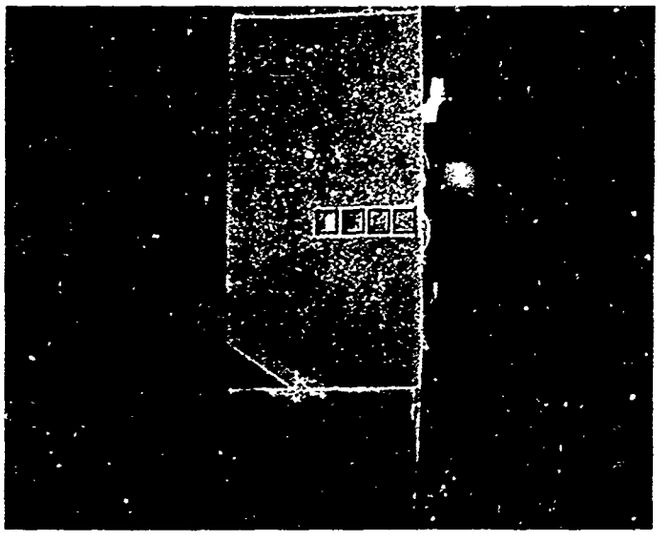

FIG. 11. TRANSDUCERS INSTALLED IN THE WHEEL
TOP VIEW

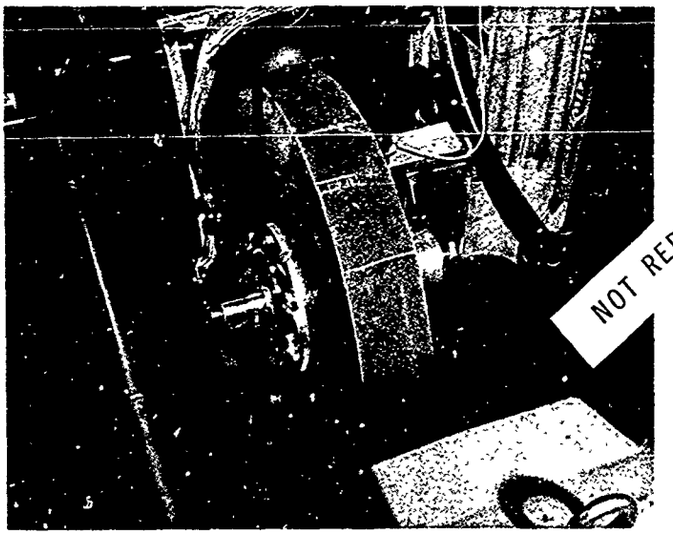

FIG. 12. GENERAL VIEW OF WHEEL
AND SLIP RING

gauges from the abrasive effects of the sand. At last this objective was achieved by coating the gauges with an anti-abrasive spray, and leaving the gaps open but providing channels into the wheel to drain the sand from the transducer pocket.

In order to connect the rotating transducers to the fixed recorder, the leads coming out of the transducers were attached to a slip ring, the fixed part of which was connected to cables going to the recorder (see Figure 12).

d. Recorders

The pressure and shear forces were recorded on a 8-channel recorder. On this same recorder the contact angle of the transducers with respect to B.D.C. was recorded by activating a remote event marker. A sample of these recordings is shown in Figure 13. The load, drawbar-pull, sinkage and torque were recorded on a four-channel recorder. The carriage velocity was recorded as pulses on the sinkage output, the spacing of which was compared to the time recorded.

Figure 14 shows a sample of these recordings. In the same manner, a two-channel recorder was used to measure the wheel velocity. This was done by short circuiting an unbalanced channel at regular intervals by means of a microswitch, and activated by event markers on the wheel. Comparison of the intervals with the recorded time is shown on Figure 15.

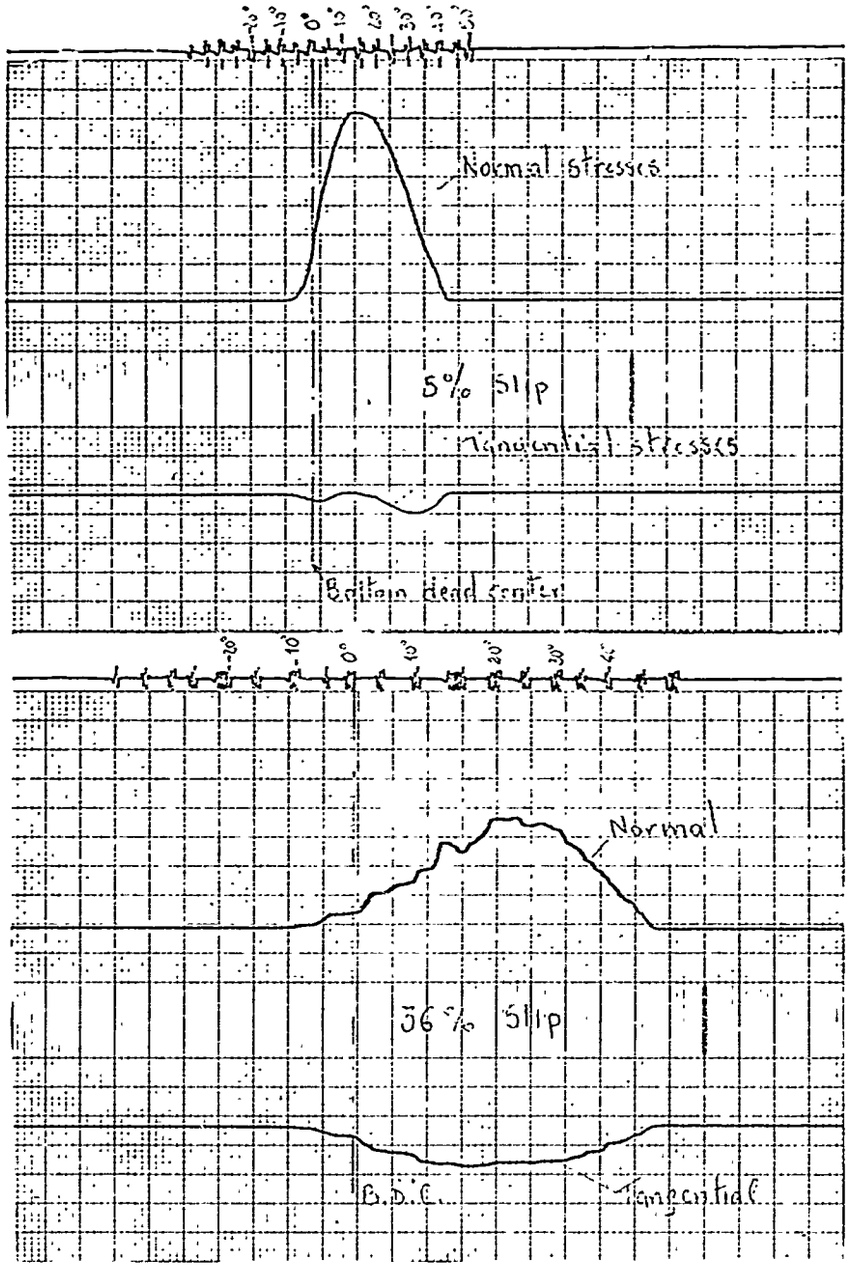

FIG. 13. SAMPLE RECORDINGS OF STRESS DISTRIBUTION

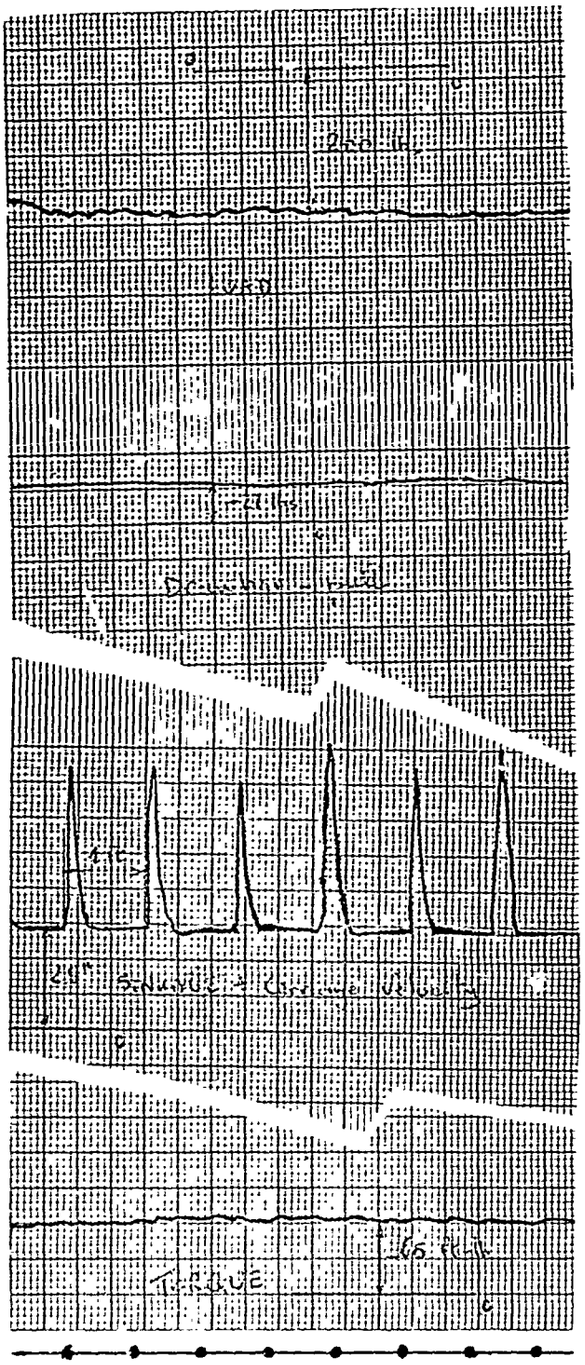

FIG. 14. SAMPLE RECORDING OF TORQUE, SINKAGE, DRAWBAR-PULL LOAD AND CARRIAGE VELOCITY

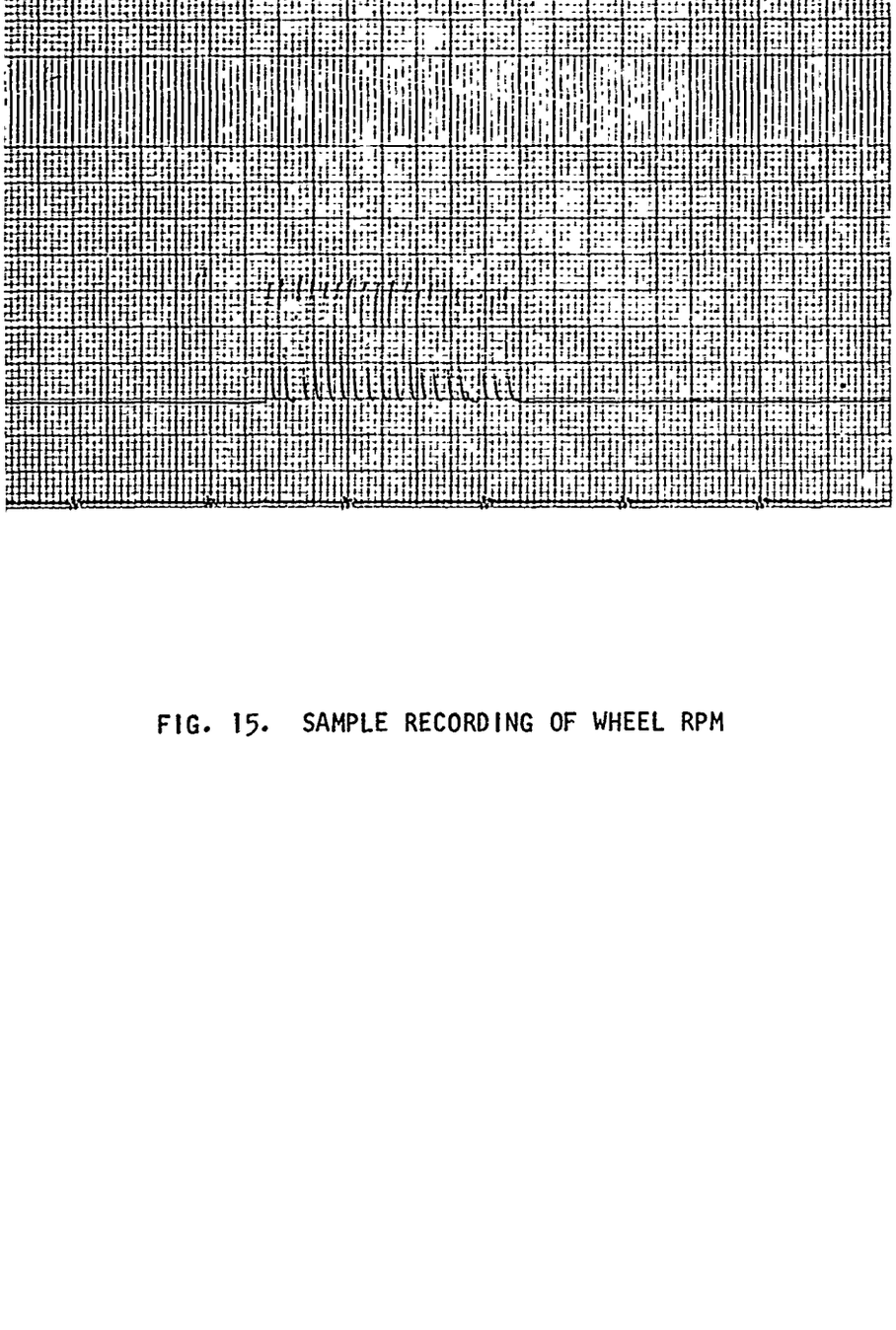

FIG. 15. SAMPLE RECORDING OF WHEEL RPM

4-4 Test Procedures

Calibration tests were conducted on all measured parameters prior to each series of tests. The wheel load gauge was statically calibrated by using a pulley and weight arrangement. Wheel torque and drawbar-pull were dynamically calibrated in order to be as close as possible to the true situation in the tests. Wheel sinkage was calibrated by sinking the wheel at one-inch increments down into the maximum depth expected.

Prior to each test run, the soil was tilled and levelled. The required wheel load was applied by filling a reservoir with air under pressure and adjusting the pressure in a second reservoir connected to the first one. The difference between pressures maintains the load fixed during the run. Prior to each run the pressures were checked and readjusted.

After the required load was applied, the carriage and the wheel drive motors were activated.

Visual observation of the data recorders indicated that the values of torque, sinkage, load and drawbar-pull stabilized in a very short distance (see Figure 14). It was therefore possible to change the carriage velocity one-third of the way through the test run and again two-thirds through the test so that three slip conditions were achieved for each run.

5. TEST RESULTS

5-1 Data

Appendix I contains the raw data from all tests conducted.

Table I - Test Results for 200 lbs load

Table II - Test Results for 350 lbs load

Table III - Test Results for 500 lbs load

Using this data the values of wheel velocity, carriage velocity and slip rate were calculated for each test condition.

Table IV - Contains the data for the stress distribution at 200 lbs

Table V - Contains the data for the stress distribution at 350 lbs

Table VI - Contains the data for the stress distribution at 500 lbs

5-2 Calculations

Wheel Velocity - Wheel velocity is defined as the tangential velocity of a point on the circumference of the wheel. This velocity was measured using a microswitch which contacted the event markers on the side of the wheel. These were fixed at 5^{o} intervals, covering an angle of 90^{o} on the side of the wheel, and measured the actual velocity of the wheel during the time the pressure cells were in contact with the sand.

To calculate the velocity, the time used by the microswitch to travel 90^{o} was multiplied by 4 to yield t_w the number of seconds required to complete a wheel revolution.

During one revolution a point on the circumference moves πD inches. Therefore, the wheel velocity, in feet per second, is calculated as:

$$V_w = \frac{\pi D/12}{t_w}$$

Carriage Velocity - Carriage velocity is defined as the velocity of a point moving with the carriage and coincident with the linear velocity of the axis of the wheel. This velocity was measured using a microswitch which contacted markers located one-foot apart along the test bin. The carriage velocity is obtained directly by comparing the number of contacts touched by the microswitch on a certain span with the time required to travel along this span.

Therefore,

$$V_c = \frac{m}{t_c}$$

Slip Rate - Slip rate is defined by and calculated from:

$$t = \frac{V_w - V_c}{V_w}$$

5-3 Graphs

Measured values of torque and drawbar-pull are plotted against the slip rate for each of the loads applied (see Figures 16, 17, 23, 24, 29, 30).

Plots of the stress distribution for variable loads and slips are given in Figures 18 through 35.

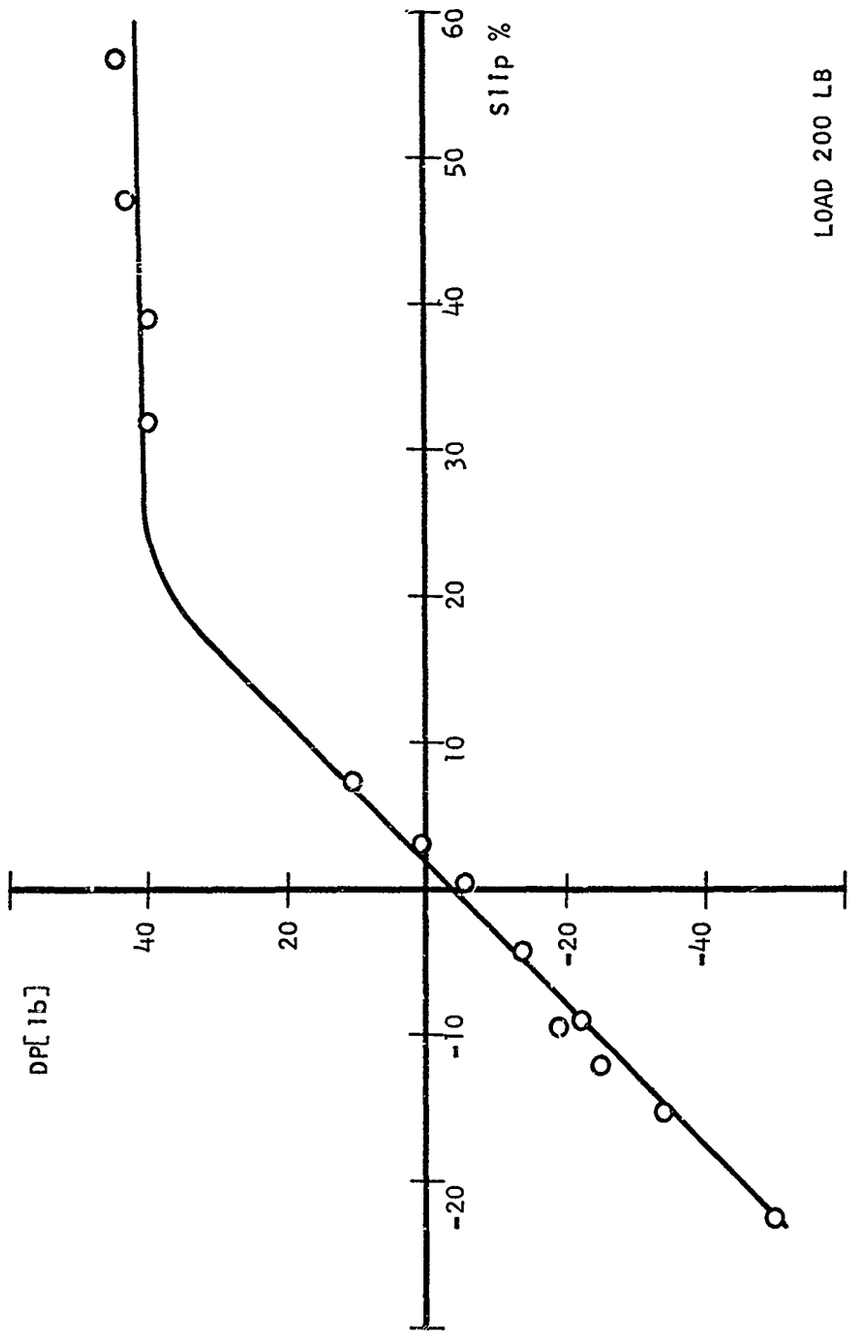

FIG.16. DRAWBAR PULL VS. SLIP

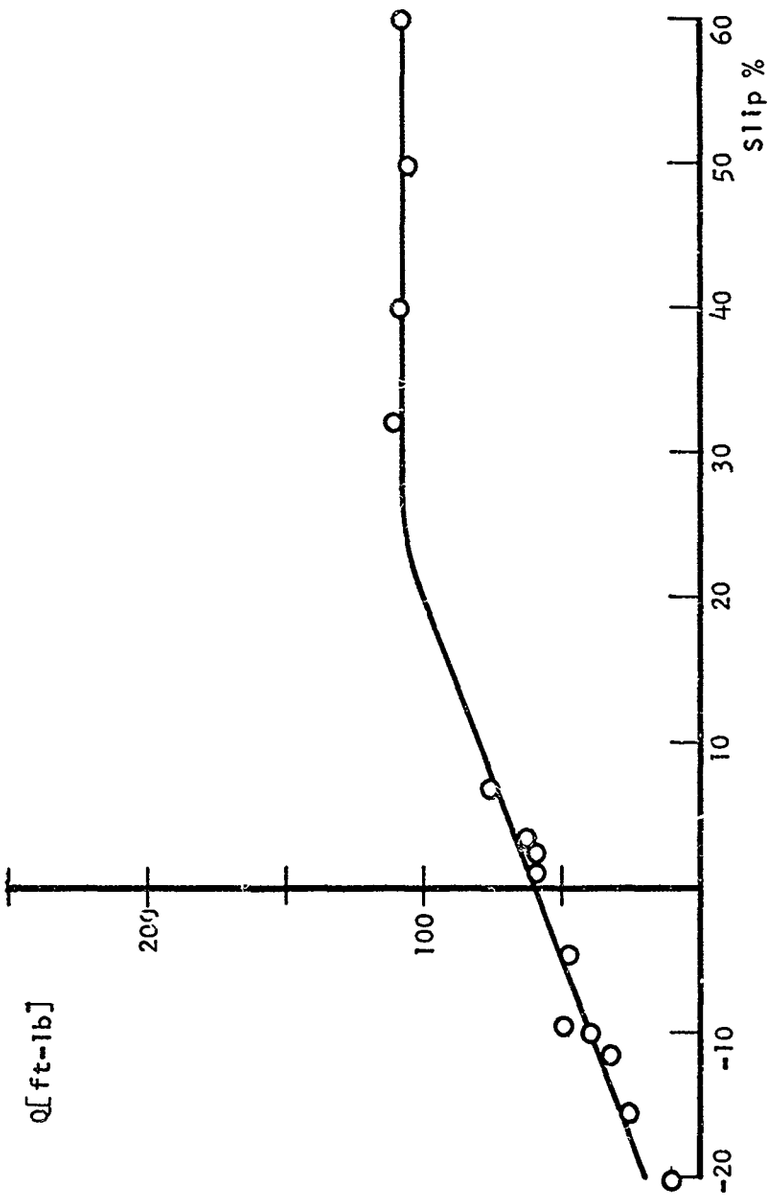

FIG. 17. TORQUE VS. SLIP

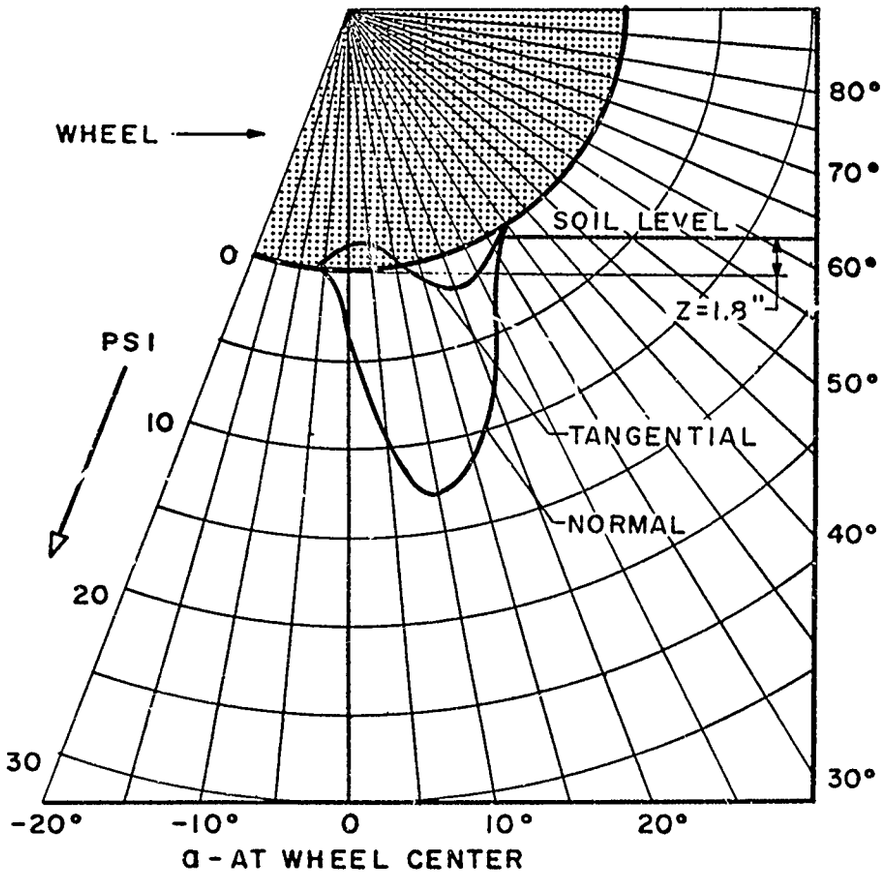

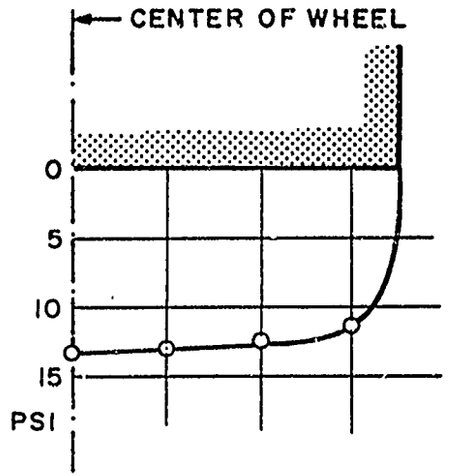

b - LATERAL DISTRIBUTION OF RADIAL STRESSES ACROSS WHEEL WIDTH

LOAD 200 LBS
SLIP - 20.5 %

FIG. 18. MEASURED STRESS DISTRIBUTION

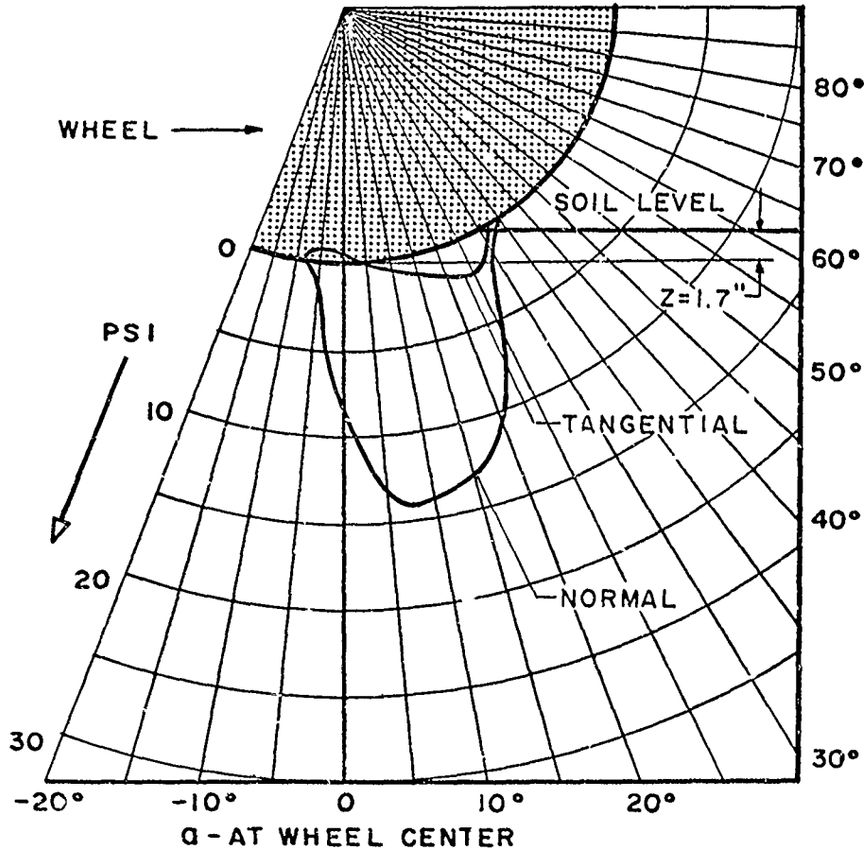

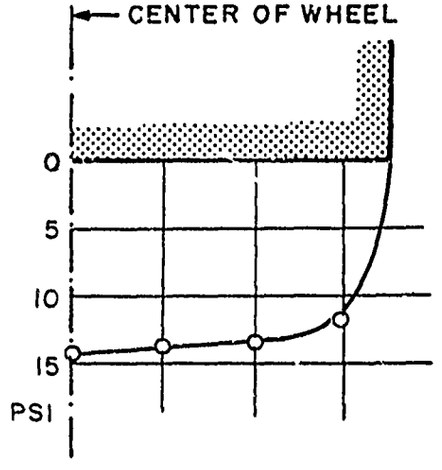

b - LATERAL DISTRIBUTION OF RADIAL STRESSES ACROSS WHEEL WIDTH

LOAD 200 LBS
SLIP -9.6 %

FIG. 19. MEASURED STRESS DISTRIBUTION

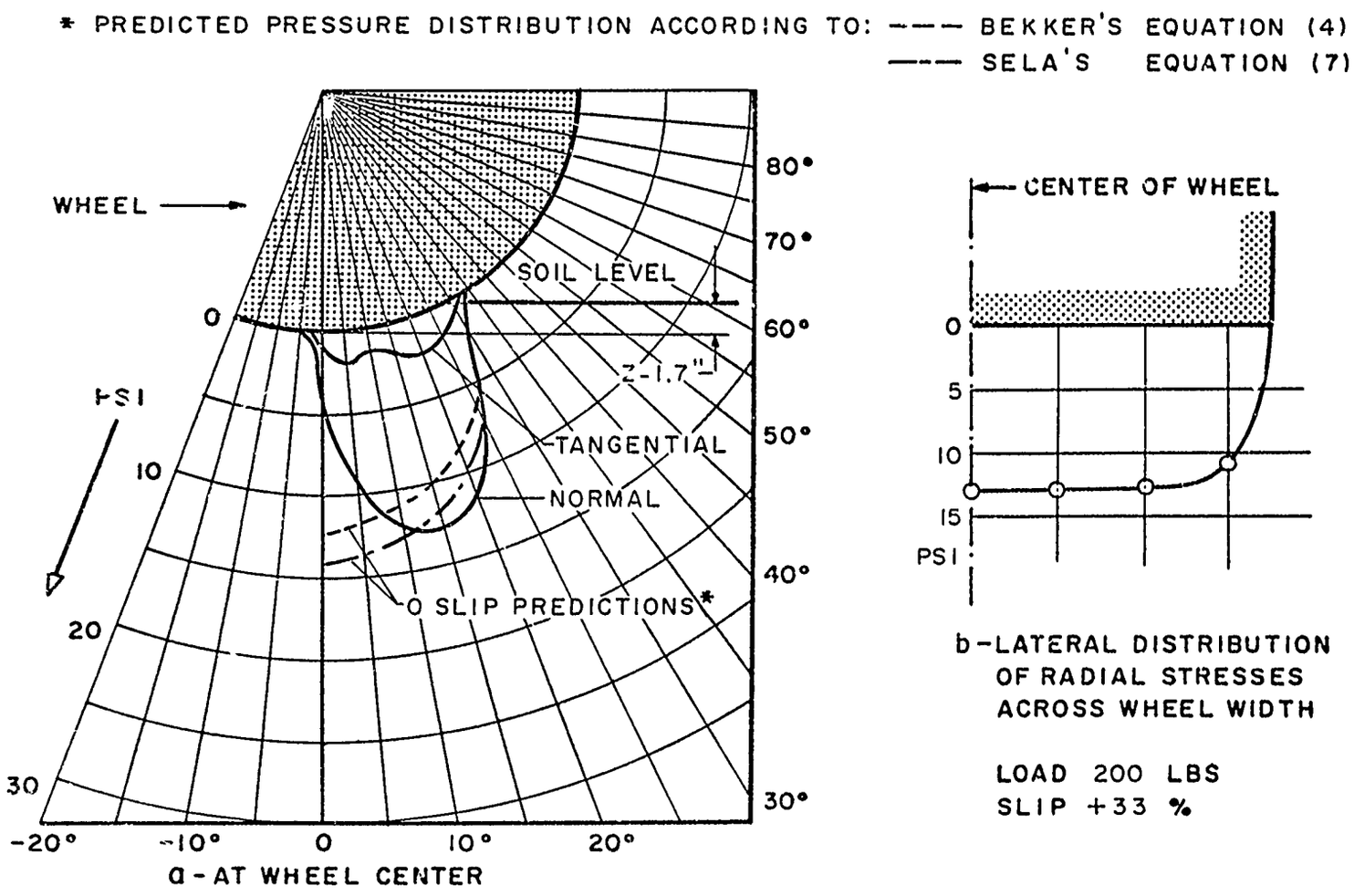

FIG. 20. MEASURED STRESS DISTRIBUTION

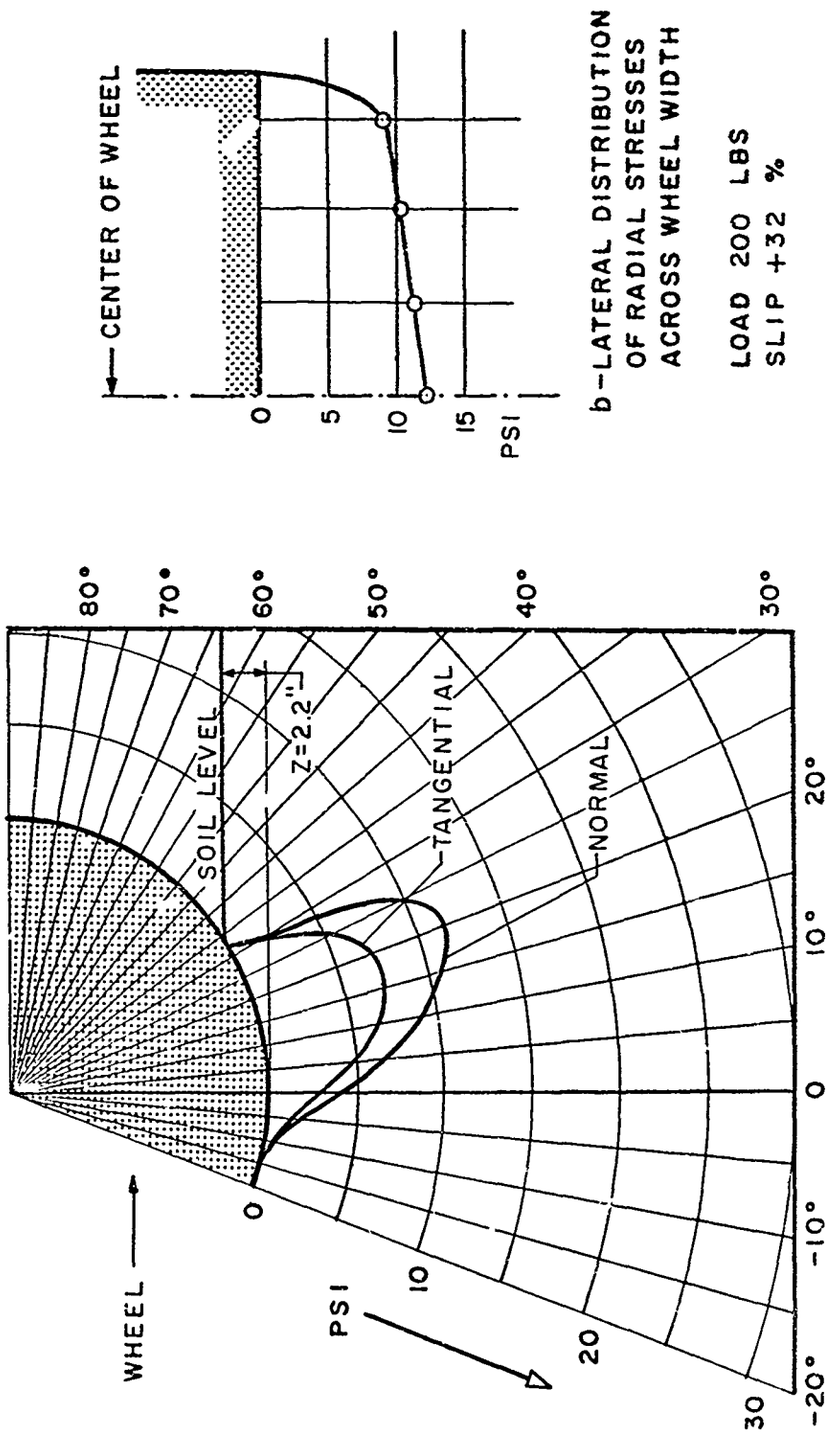

FIG. 21. MEASURED STRESS DISTRIBUTION

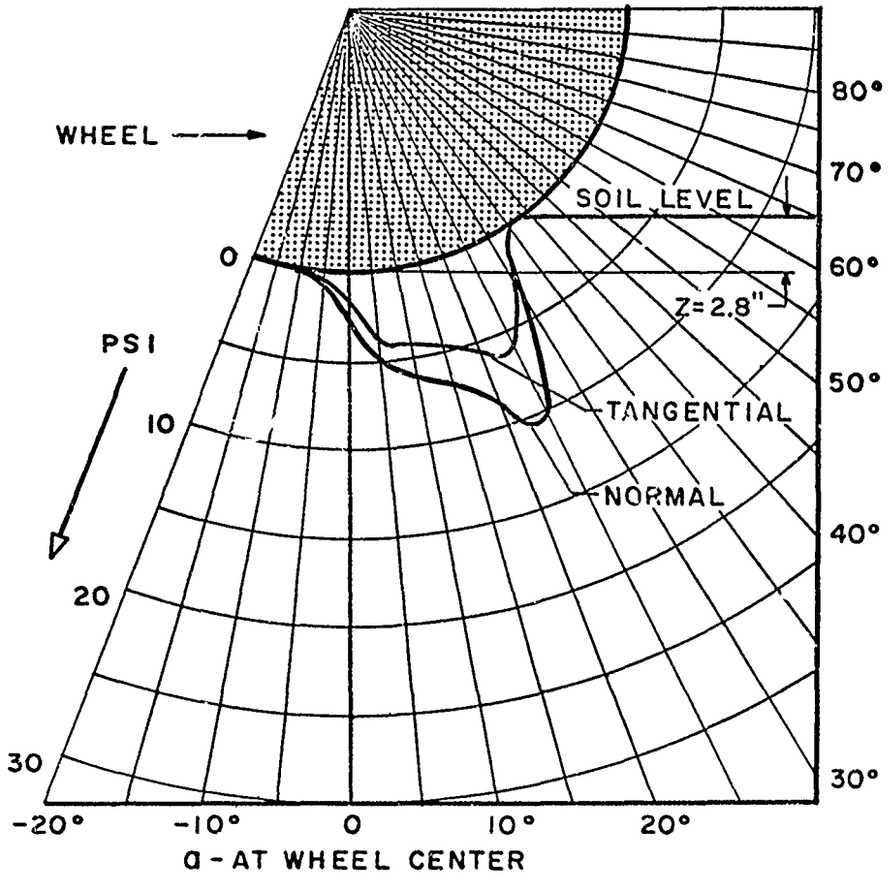

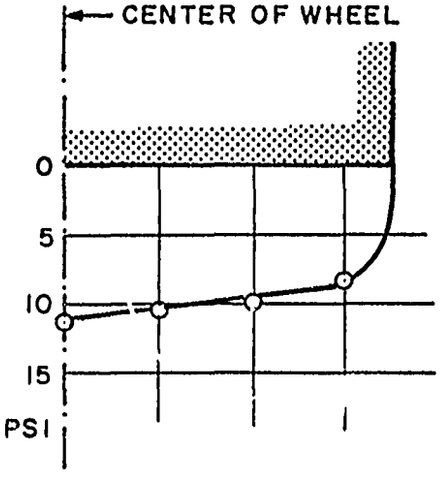

b - LATERAL DISTRIBUTION OF RADIAL STRESSES ACROSS WHEEL WIDTH

LOAD 200 LBS
SLIP + 52 %

FIG. 22. MEASURED STRESS DISTRIBUTION

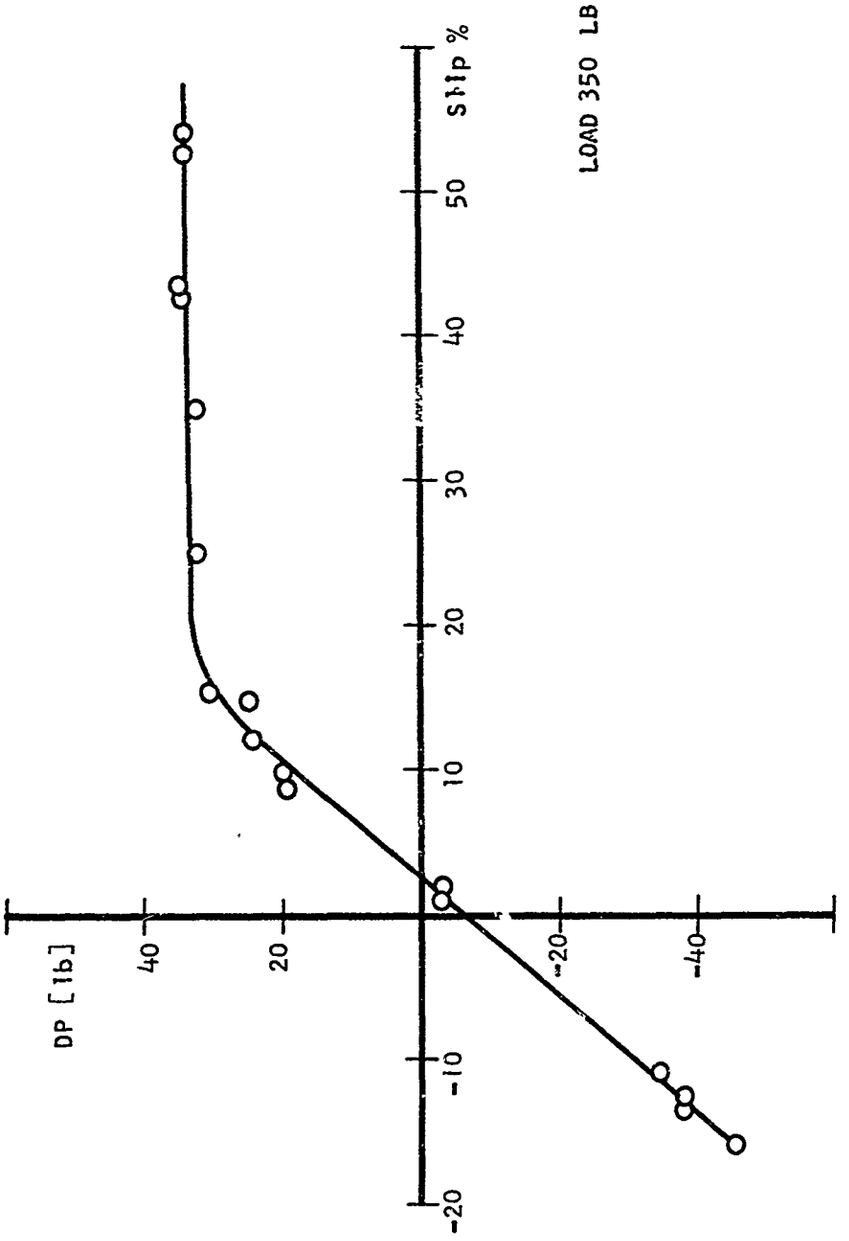

FIG. 23. DRAWBAR-PULL VS. SLIP

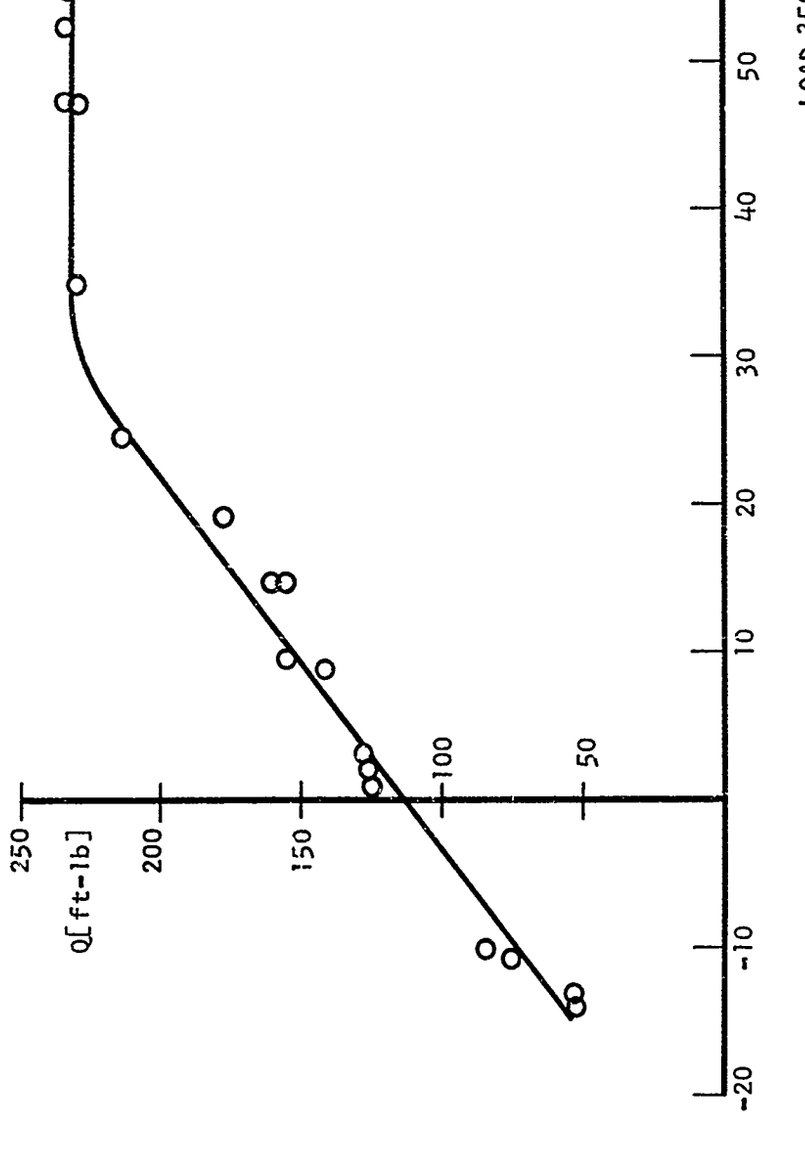

FIG. 24. TORQUE VS. SLIP

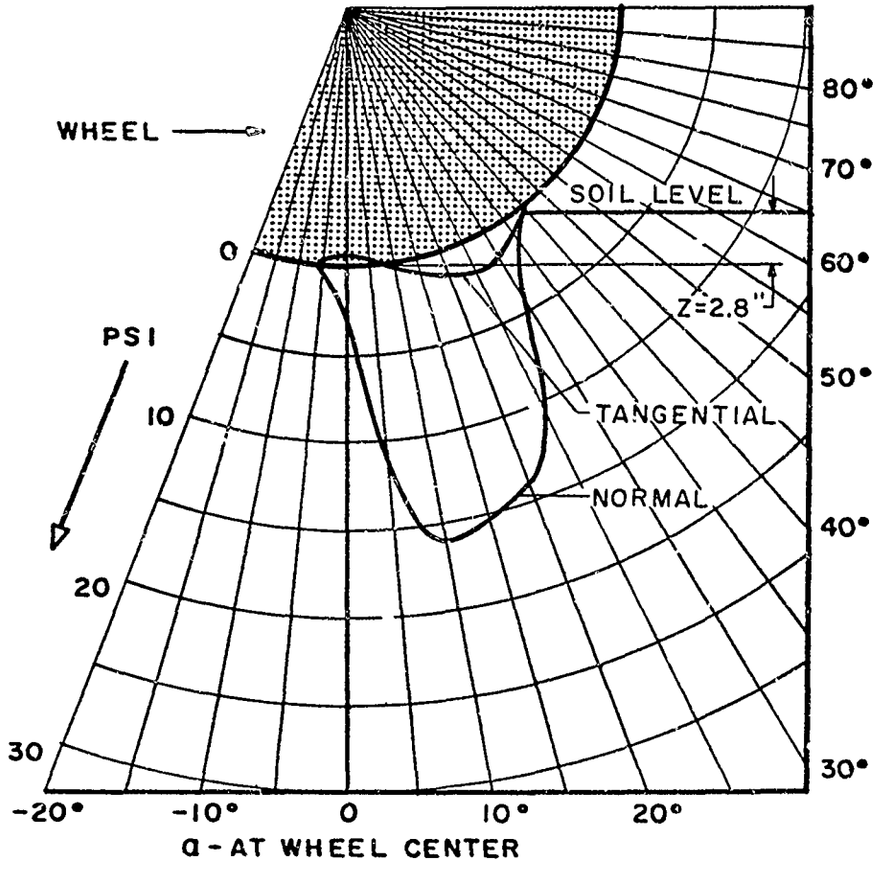

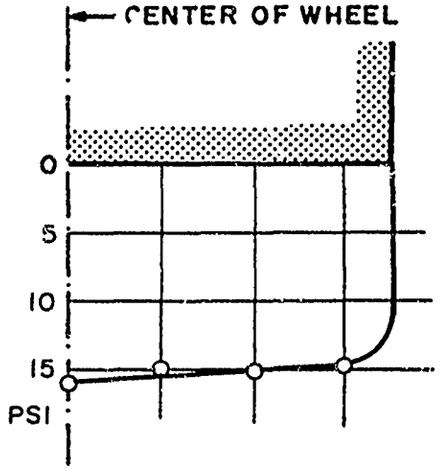

b - LATERAL DISTRIBUTION OF RADIAL STRESSES ACROSS WHEEL WIDTH

LOAD 350 LBS
SLIP -14.5 %

FIG. 25. MEASURED STRESS DISTRIBUTION

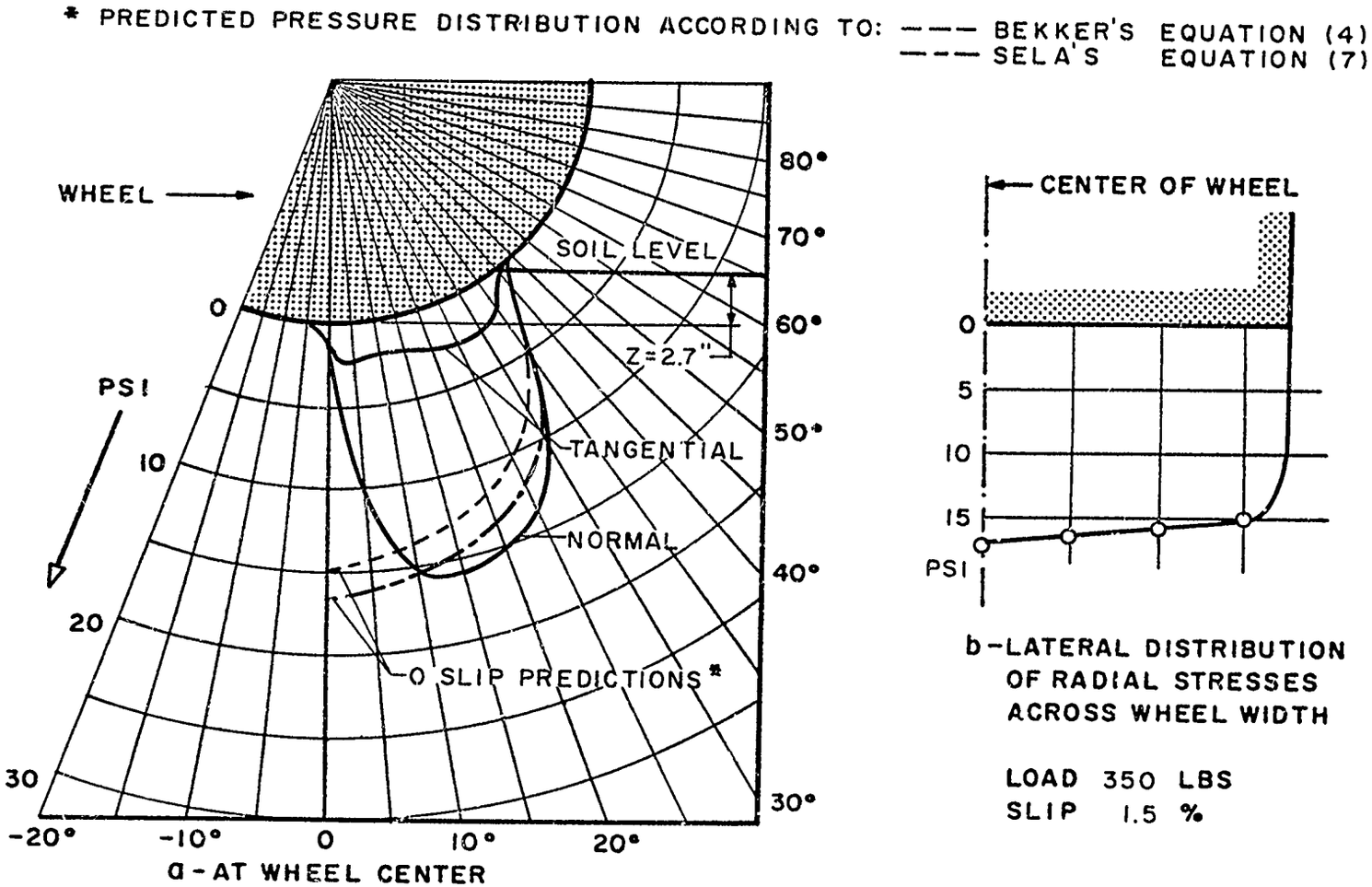

FIG. 26. MEASURED STRESS DISTRIBUTION

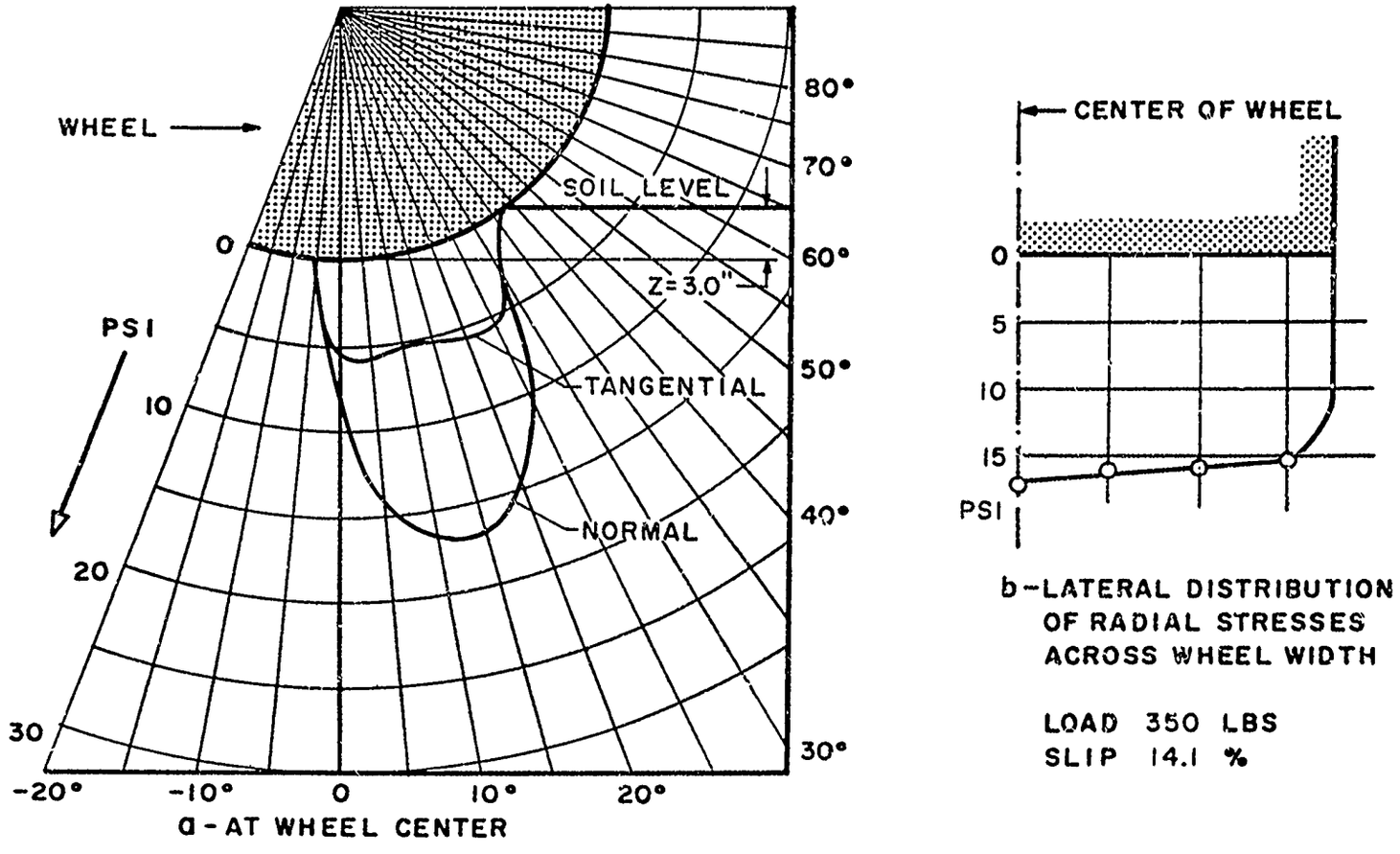

FIG. 27. MEASURED STRESS DISTRIBUTION

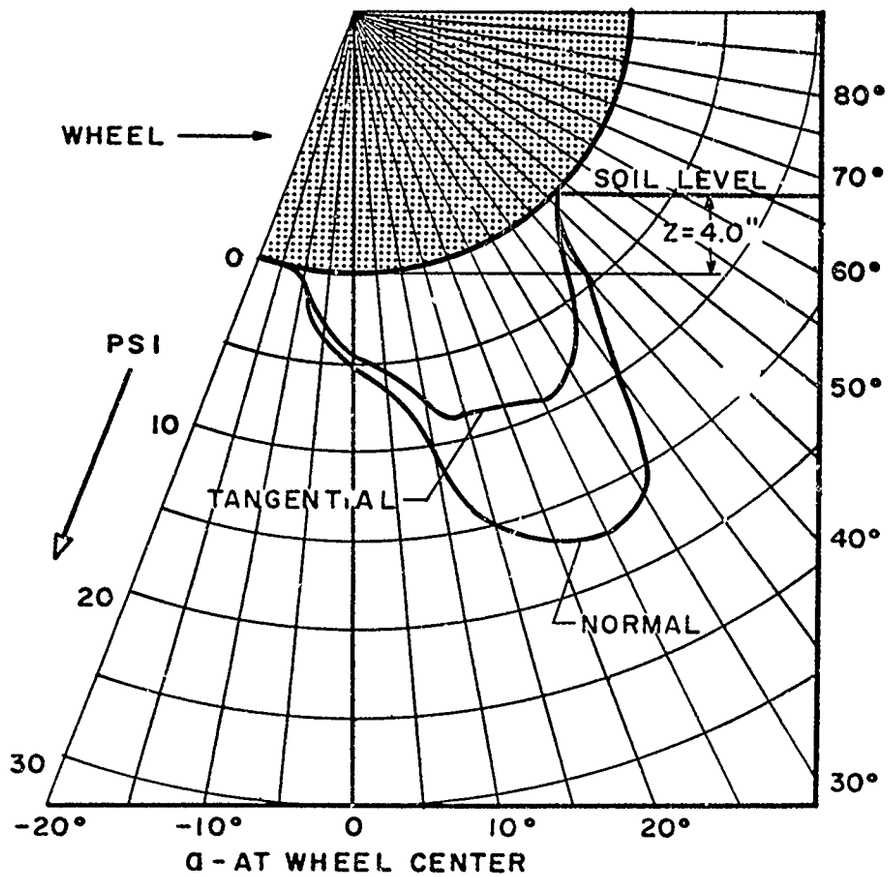

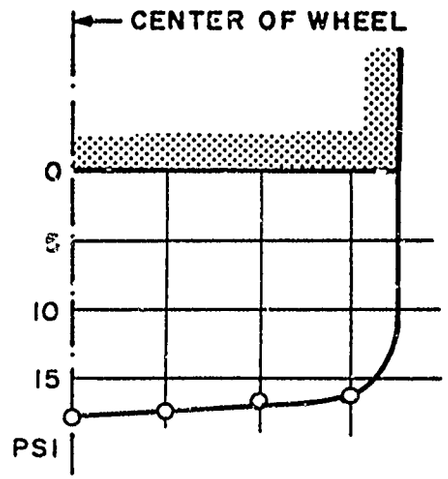

b - LATERAL DISTRIBUTION OF RADIAL STRESSES ACROSS WHEEL WIDTH

LOAD 350 LBS
SLIP 45 %

FIG. 28. MEASURED STRESS DISTRIBUTION

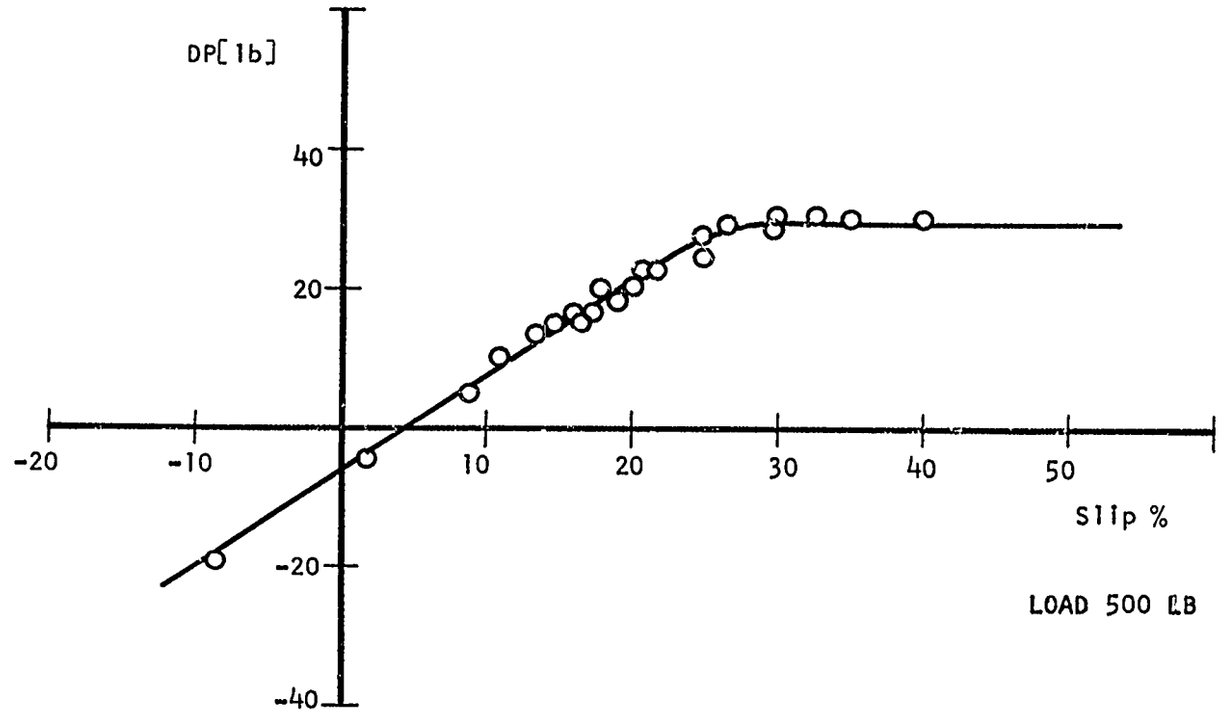

FIG. 29. DRAWBAR-PULL VS. SLIP

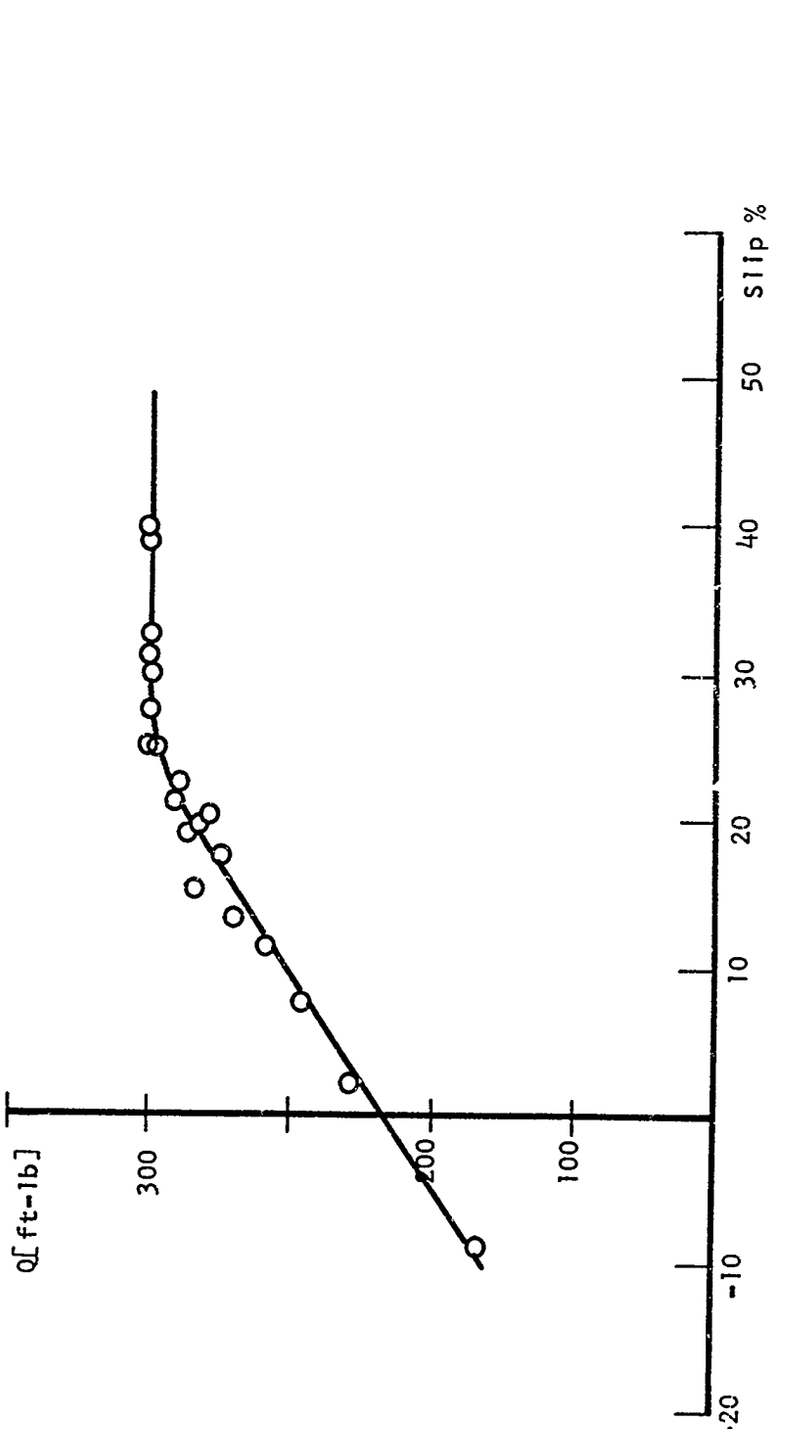

FIG. 30. TORQUE VS. SLIP

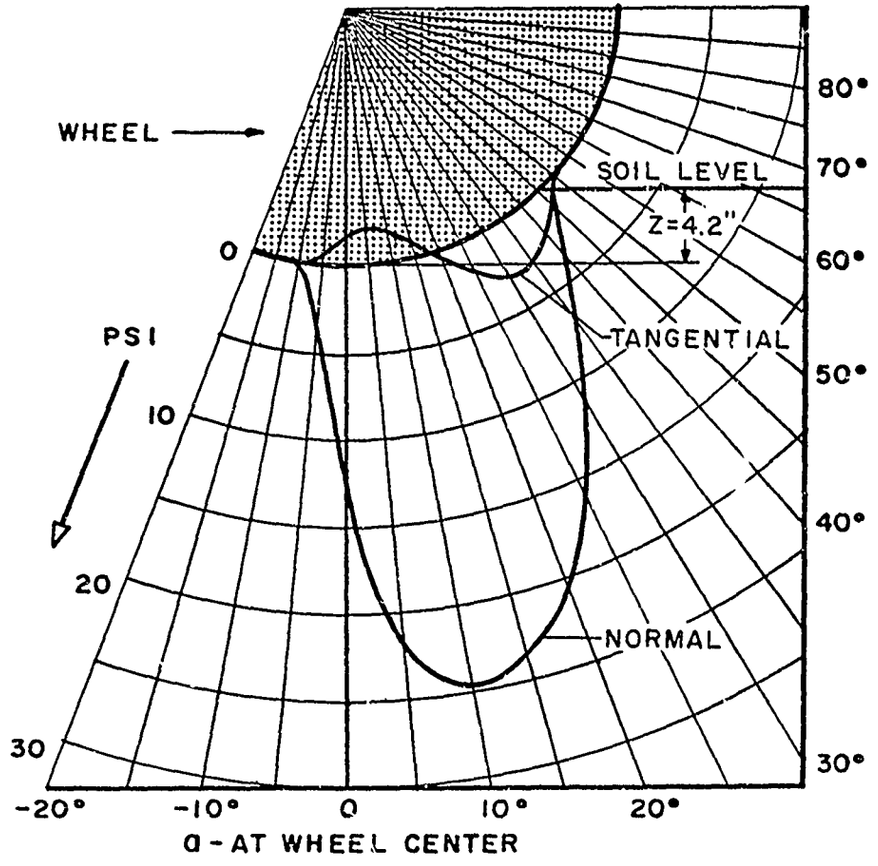

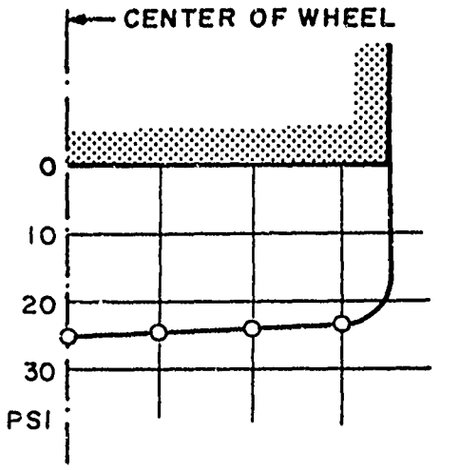

b - LATERAL DISTRIBUTION OF RADIAL STRESSES ACROSS WHEEL WIDTH

LOAD 500 LBS
SLIP -9.5 %

FIG. 31. MEASURED STRESS DISTRIBUTION

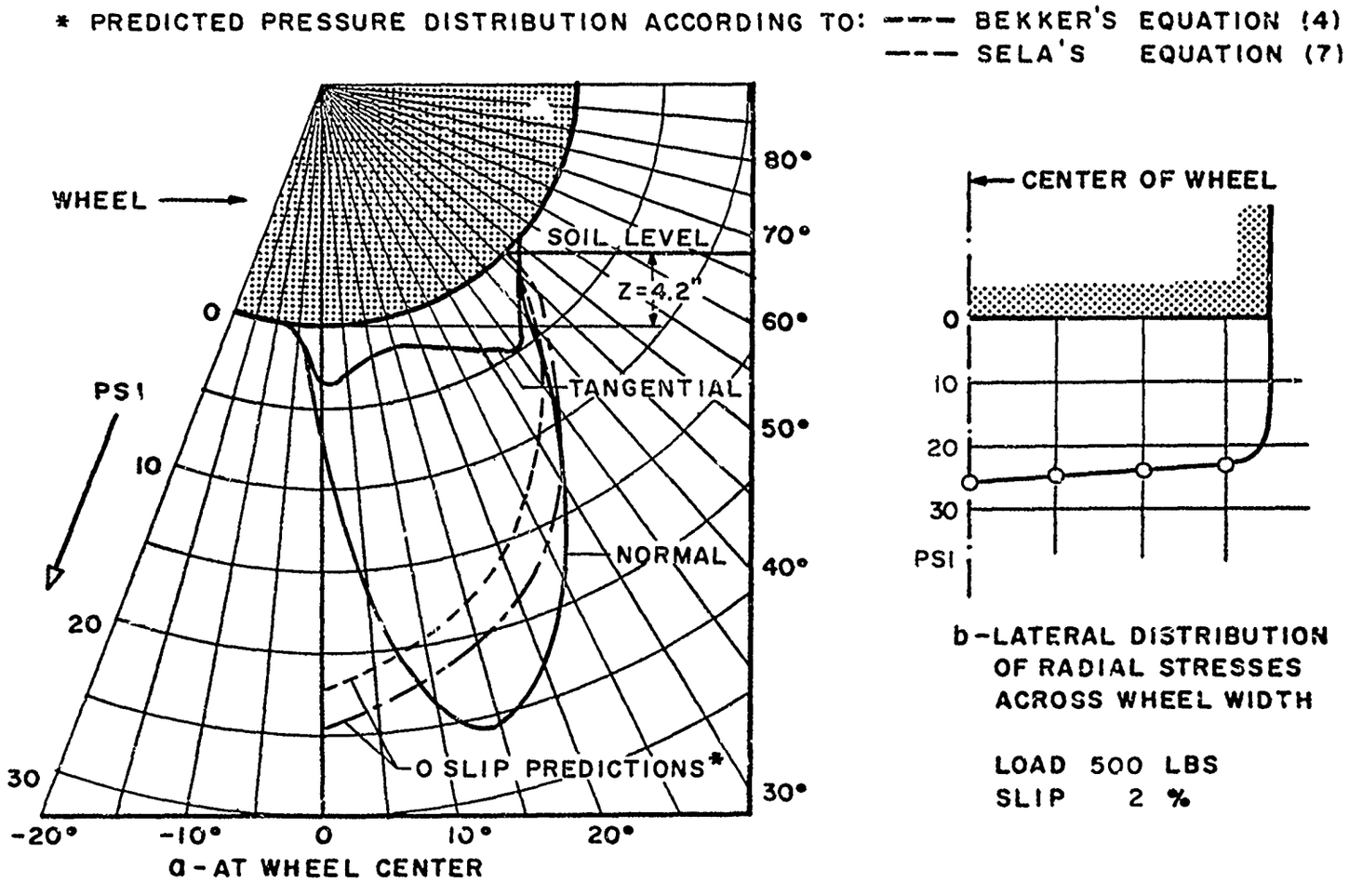

FIG. 32. MEASURED STRESS DISTRIBUTION

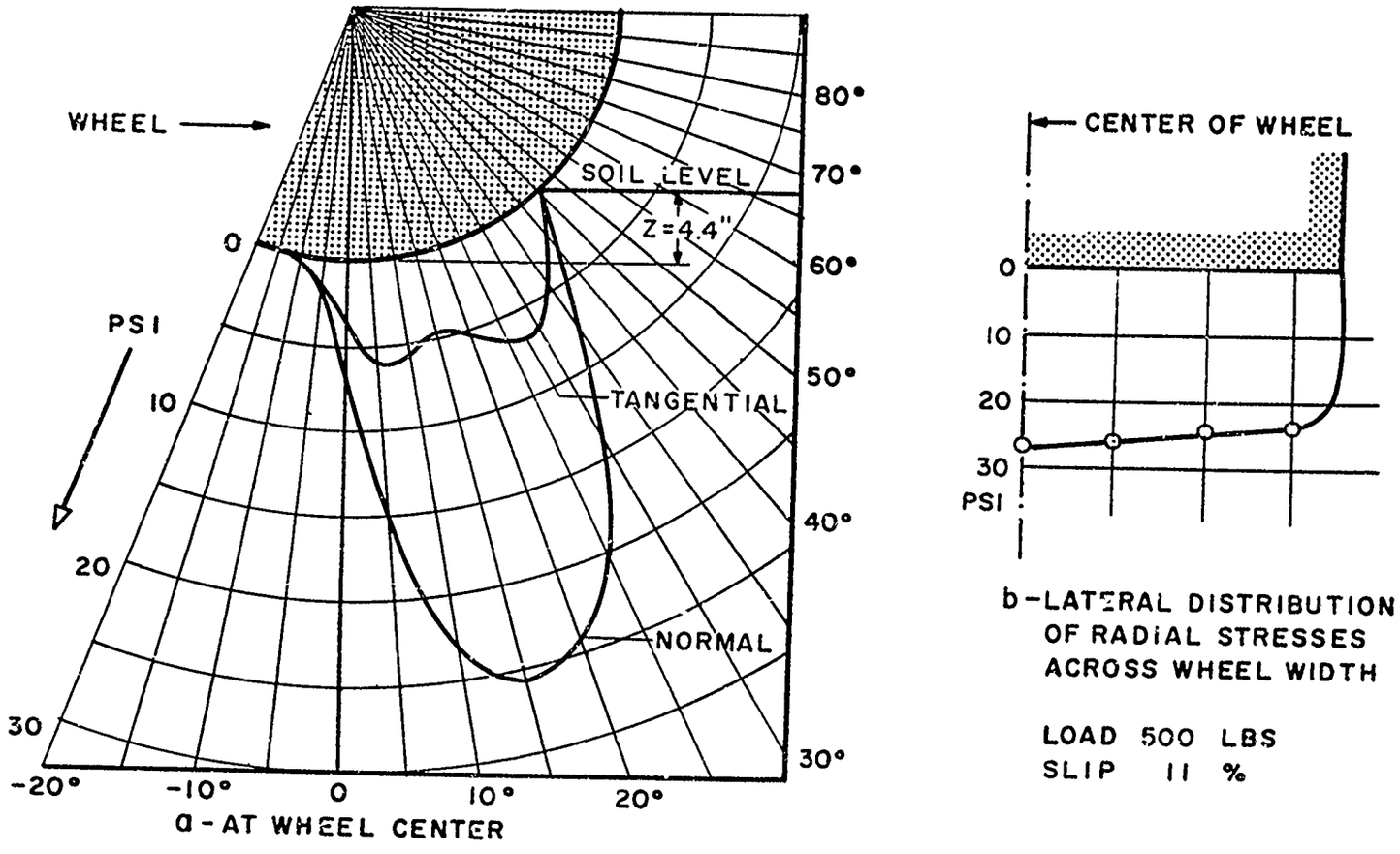

FIG. 33. MEASURED STRESS DISTRIBUTION

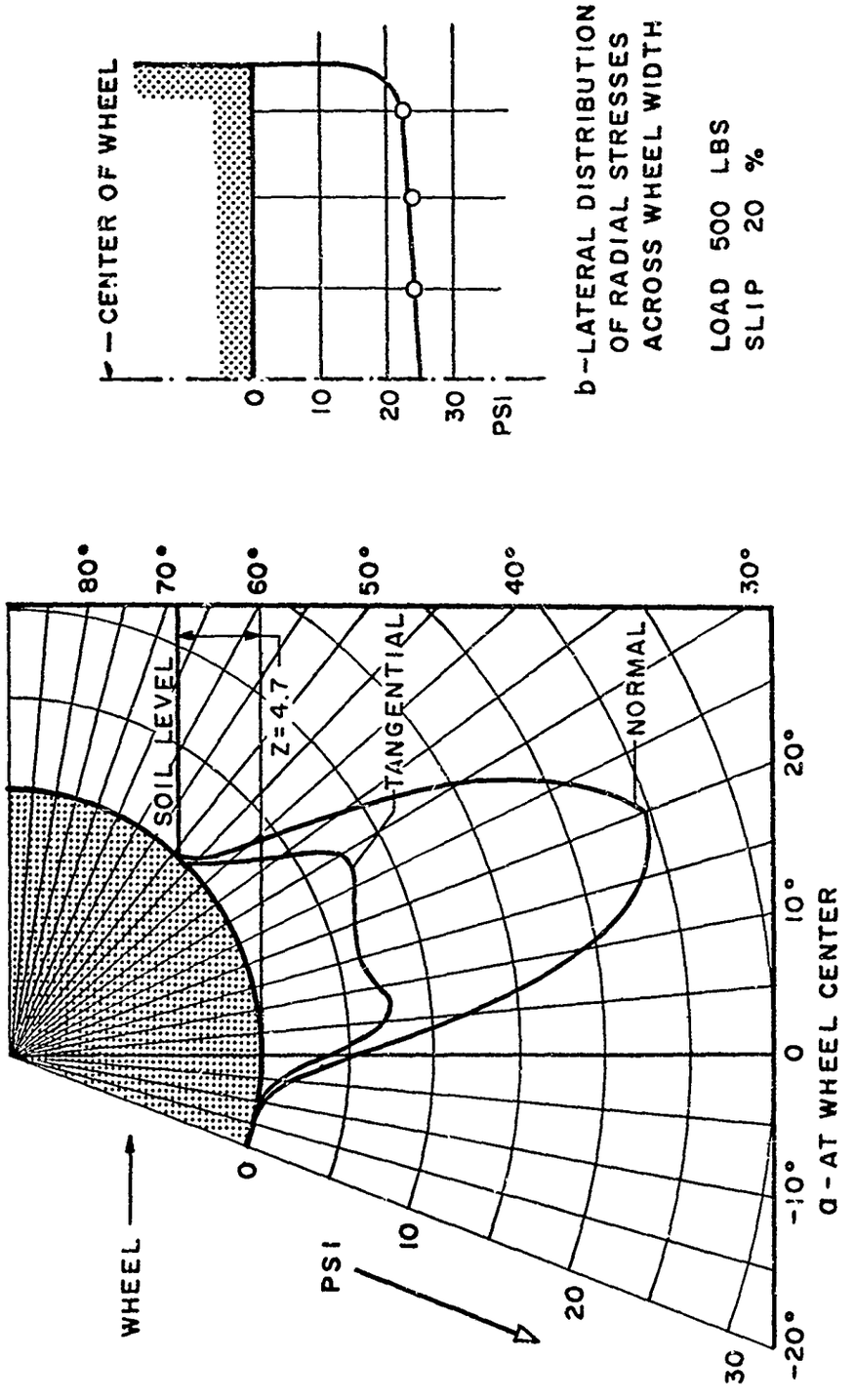

FIG. 34 MEASURED STRESS DISTRIBUTION

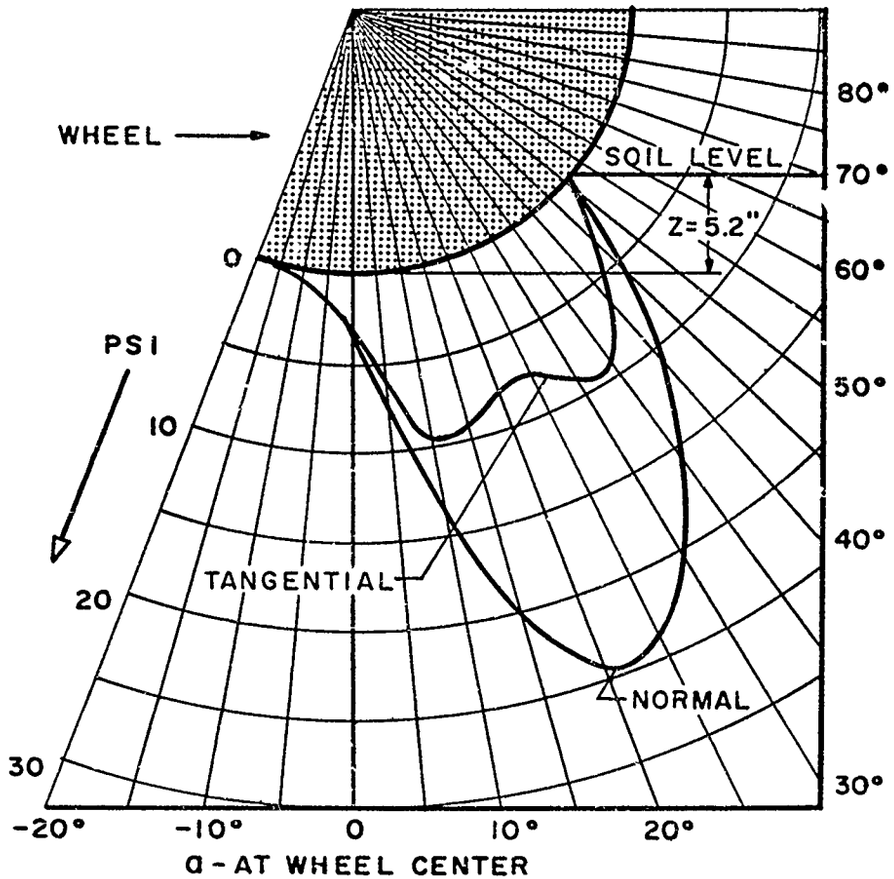

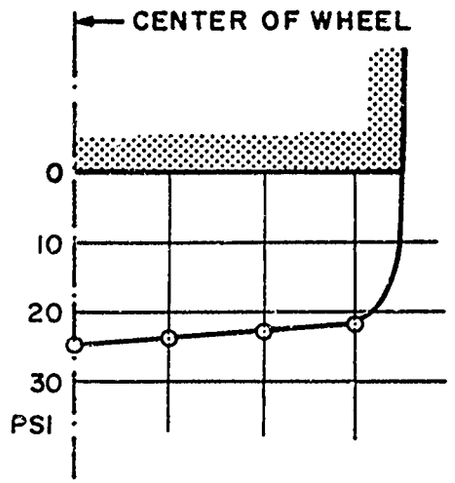

b - LATERAL DISTRIBUTION OF RADIAL STRESSES ACROSS WHEEL WIDTH

LOAD 500 LBS
SLIP 38 %

FIG. 35. MEASURED STRESS DISTRIBUTION

6. DISCUSSION OF RESULTS

6-1 Validation Check

To check the accuracy of the stress measurements, the data for the stresses was integrated according to Equations (1) and (3). Then these results were compared to the external forces:

$$W = b\frac{D}{2}\int_{\alpha_2}^{\alpha_1} p(\alpha)\cos\alpha d\alpha + b\frac{D}{2}\int_{\alpha_2}^{\alpha_1} s(\alpha)\sin\alpha_o d\alpha \qquad (1)$$

$$Q = b(\frac{D}{2})^2\int_{\alpha_2}^{\alpha_1} s(\alpha)\, d\alpha \qquad (3)$$

Graphical techniques were used for the integrations. For every slip, plots of $p\cos\alpha$ vs α, $s\sin\alpha$ vs α, and s vs α were drafted. Then the area under the graph was calculated, multiplied by the respective factor($b\frac{D}{2}$, $b(\frac{D}{2})^2$) and summed according to Equations (1) and (3). (Mean values of p and s were used over the wheel width.)

Plots of the torque and load vs slip drawn according to the integrations and the measured forces are shown in Figures 36 through 39.

As seen from the plots, the results for the torque agree closely, while the integrated values for the load yield values 10% higher than the measured load in the high slip range. This may be attributed to the fact that the readings were affected by the bouncing of the wheel at high slip rates and the curves had to be smoothed to perform integration (an example of such a reading is given in Figure 40). Besides the measured load is an average value, while the measured stresses are instantaneous. Thus the comparison is difficult. At

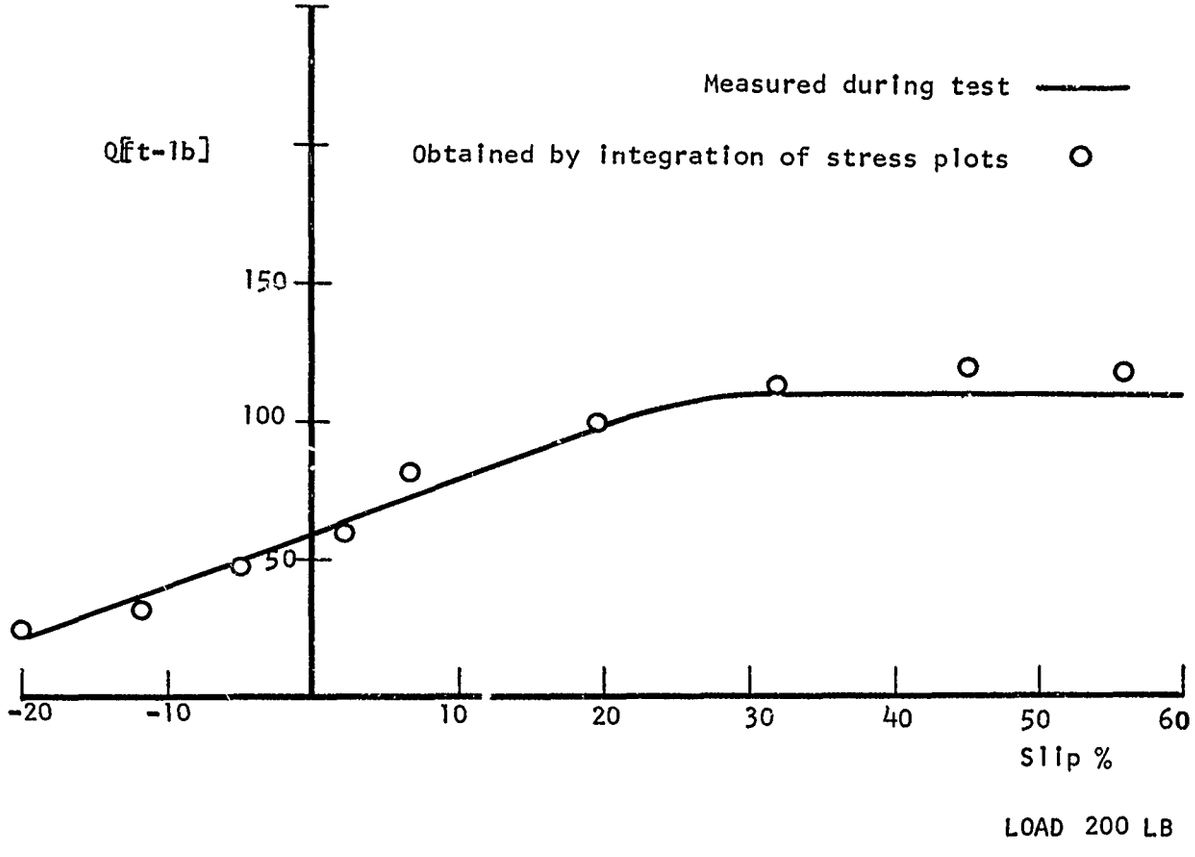

FIG. 36. TORQUE VS. SLIP

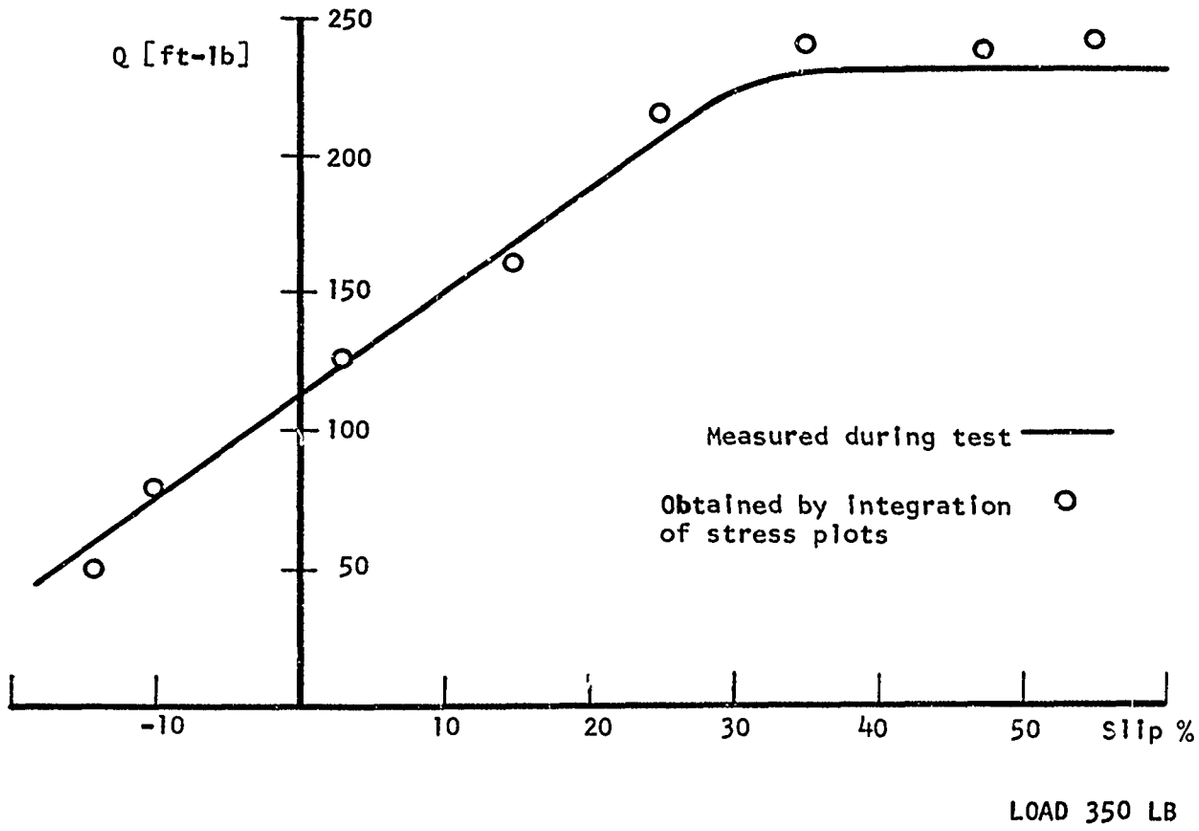

FIG. 37. TORQUE VS. SLIP

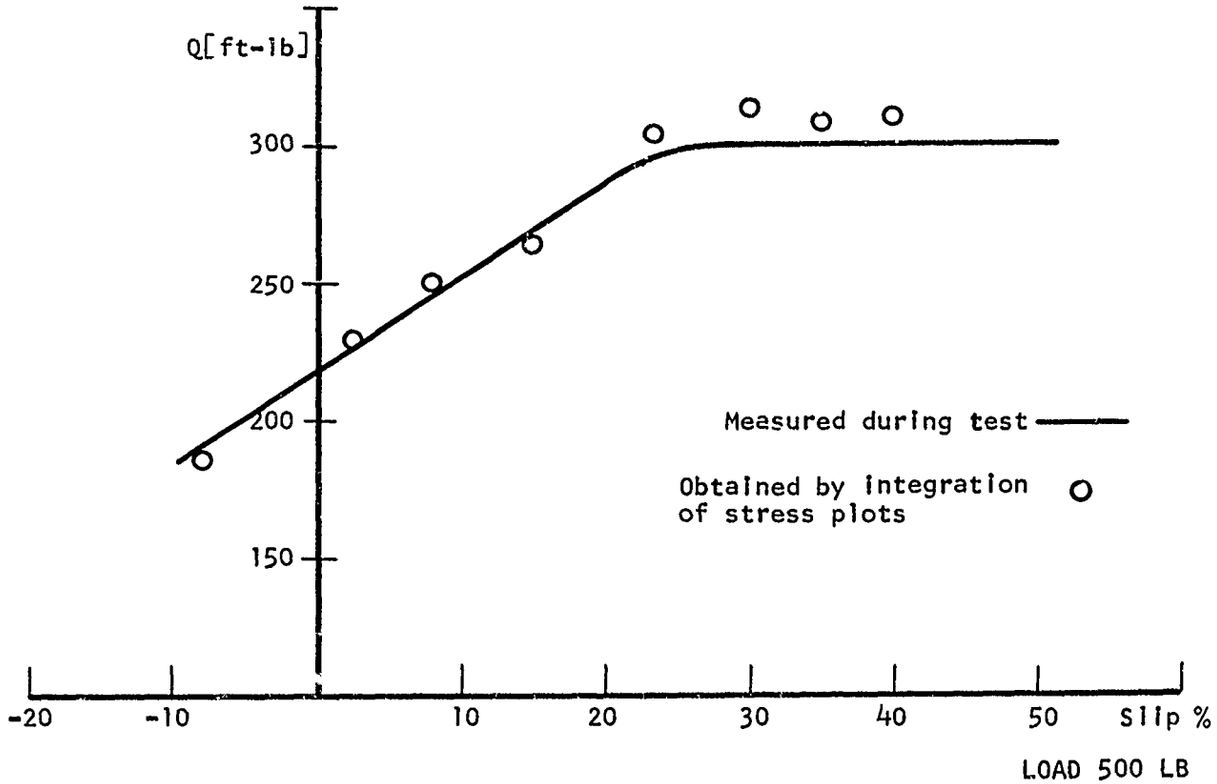

FIG. 38 TORQUE VS. SLIP

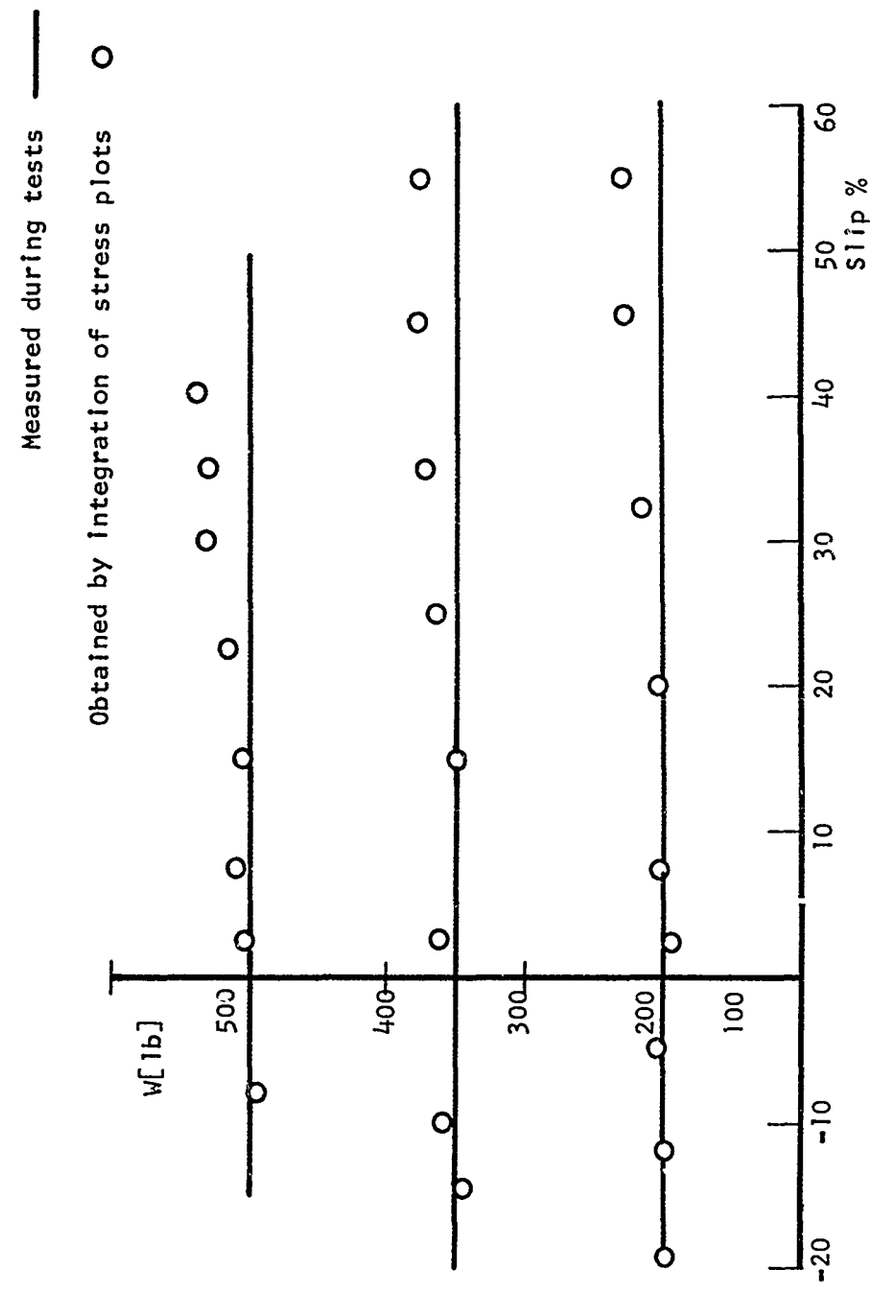

FIG. 39. LOAD VS. SLIP

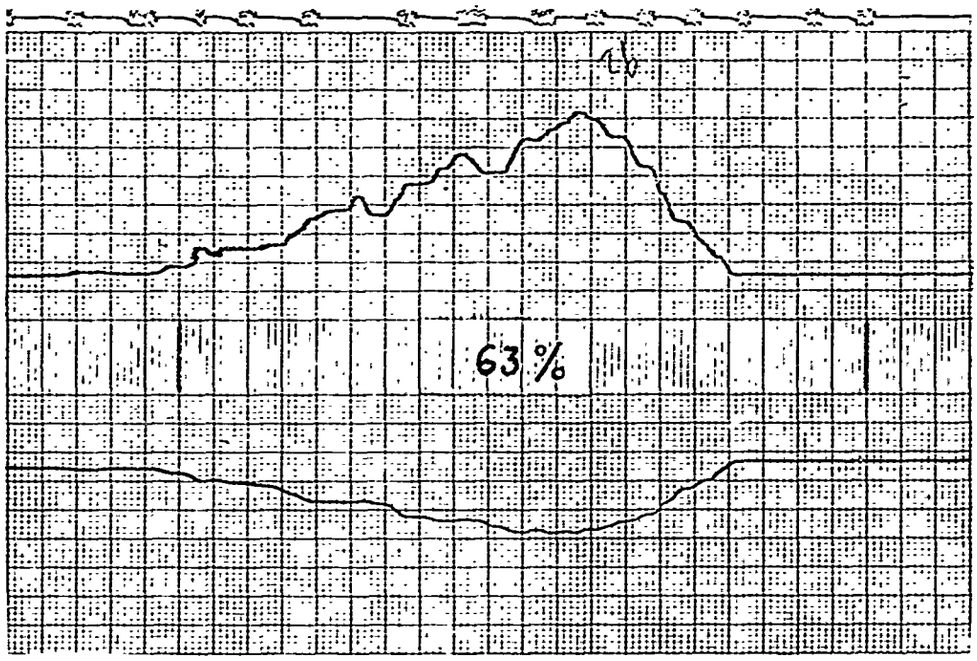

FIG. 40. SAMPLE RECORDING OF STRESSES AT HIGH SLIP

high slips the changes in load are as large as ±30 lbs.

6-2 Comparison with Prediction Equations

Figures 20, 26, and 32 show a comparison of measured and predicted pressure distribution near zero slip. Sela's Equation (7) yields a curve closer to the measured one than does Bekker's Equation (4). However, the pressure predicted by both equations deviates significantly from the measured pressure in the region $\alpha = 0$. Actually they predict a maximum pressure where it is close to nil.

Taking this into consideration, Sela[7] in computing the performance of the wheel, neglects the load supported by the shear stresses, thus compensating for the excess area under the curve.

One of the objectives of this thesis was to check this assumption. Figure 41 shows a comparison of the load supported by the shear stresses area (1) to the load supported by the excess area (2) under the prediction curves as given by Equation (7). Although the shear stresses area (1) is much smaller than the excess area (2), this difference is compensated for by areas (3) and (4) which are not included in the prediction graph.

We see then, that near zero slip predictions based on Equation (7) assuming that all the load is supported by the normal pressure are valid, with 6% error at the most.

6-3 Stress Behavior

Figures 18 through 36 show graphs of radial and shear stress distribution for each of the three loads. For every load, representative graphs of the series of tests are shown. One is for the towed

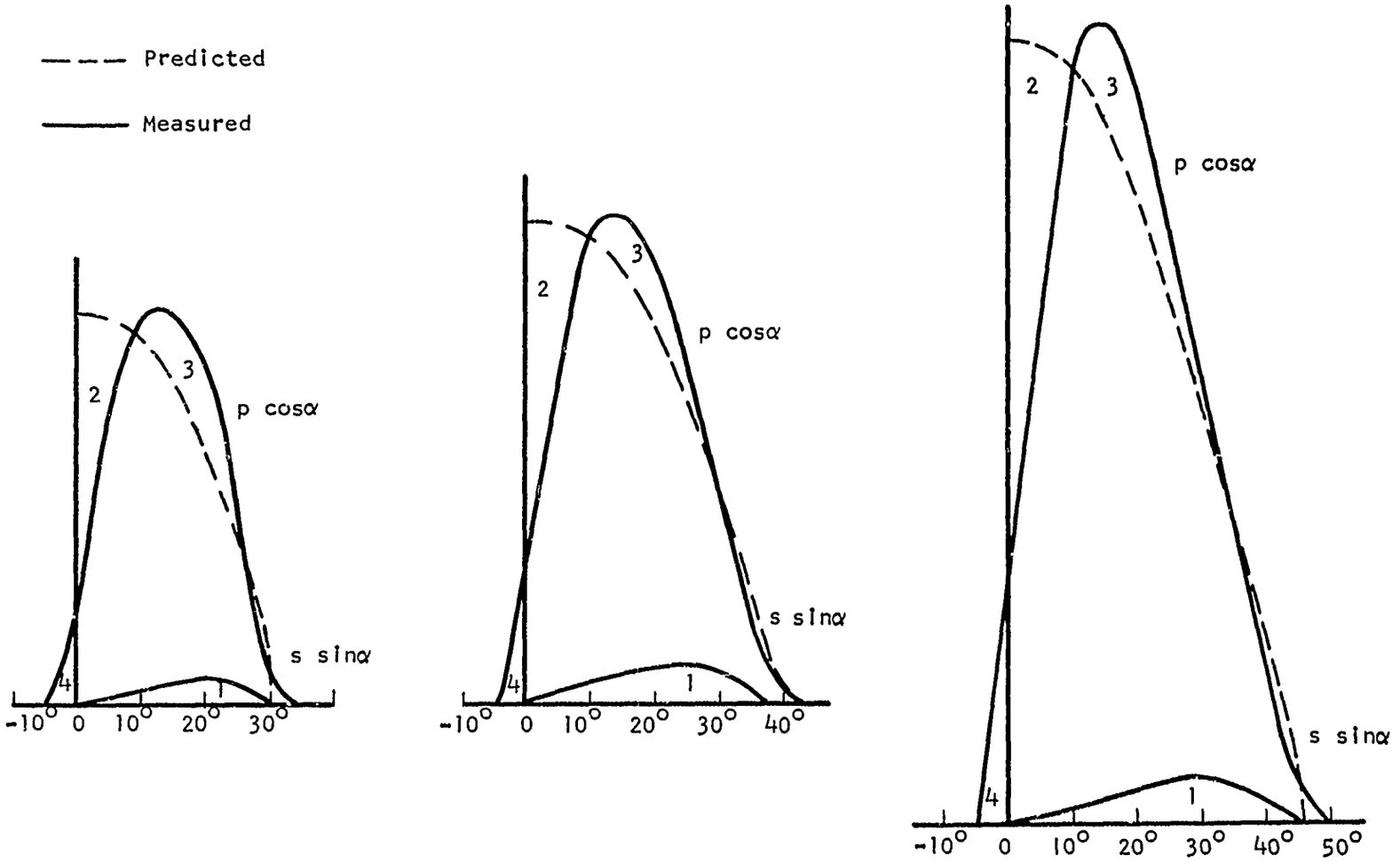

FIG. 41. COMPARISON OF PREDICTIONS BY SELA WITH MEASURED STRESSES

wheel (negative slip) one near the self-propelled point, and the other at medium and large slip rates. On some of the graphs (near zero slip) predicted distributions are shown.

Obviously, the radial pressure distribution deviates from the predictive equation and the deviation grows larger with increasing slip.

The measured pressure is more symmetrical in shape than the predictive equations and the maximum pressure occurs well forward of bottom dead center. This peak moves forward with increasing slip.

The shear stresses increase with slip and the ratio of shear to normal stresses becomes as high as 60% for high slips. On the other hand, the pressure decreases with slip.

At all positive slips the tangential stresses are positive, although they show a minimum at the same angle the radial stress is at a maximum.

Near zero slip the shear stresses are still positive. When negative slip occurs (towed wheel) a zone of negative shear develops at the rear of the contact surface. At zero torque, the negative and positive slips are equal.

The lateral distribution shows only slight changes with slip or load. It always shows a loss of strength at the edge of the wheel, while along the wheel width it is more or less constant. At the center, it is slightly higher and for high slips the loss of strength begins at the center. The change in wheel load changes the pressure values, but the general form of the curve remains unchanged.

7. CONCLUSIONS

The results of these tests lead to the following conclusions about the prediction of wheel performance:

(1) The basic assumption that the radial stresses beneath a rigid wheel are equal to the pressure beneath a strip footing of the same width at the same depth is not generally true. The actual stress distribution has its peak value forward of bottom dead center and this moves further forward with increasing slip.

(2) However, for zero slip (or near it) Sela's Equation (7) can be used with good accuracy.

From the good correlation given by the results of these tests, we may conclude that the equipment built for this study served its purpose very well. Good results were yielded by the dynamometer, although some of its components, which would have given even more accurate results, were not completely assembled. The transducers were very sensitive and gave a better performance than expected.

8. RECOMMENDATIONS

1. To complete this study, we recommend that some tests be conducted in cohesive soils and soils with both cohesion and friction.

2. In order to get better performance predictions, any equation describing radial pressure distribution has to be a function of slip.

3. A comprehensive shear stress-slip theory which takes into account the soil flow should be developed to fill the gap left open in soil-vehicle system analysis.

9. ACKNOWLEDGEMENTS

This study was performed under the Department of Defense Themis Project (Contract DAAE 07-69-C-0356) in the new dynamometer facility and soil bin of Davidson Laboratory.

First, I wish to thank Colonel A. D. Sela, Ordnance Corps. Israeli Army, who made possible my stay in the United States. He proposed this project and made valuable suggestions and recommendations which facilitated the work.

Lt. Colonel John L. Johnsen, Armor Corps, U.S. Army, assisted in conducting the experimental tests for this study.

Dr. I. R. Ehrlich, my thesis advisor, guided and reviewed the work and edited the final manuscript.

Dr. Louis I. Leviticus made many valuable suggestions about the equipment.

Miss Dolores Pambello typed this manuscript.

I wish to express my appreciation to all these people for their help, without which, the present work would not have been possible.

10. REFERENCES

1. M.G. BEKKER, "Theory of Land Locomotion" (The Mechanics of Vehicle Mobility) University of Michigan Press, Ann Arbor, Michigan, 1956.

2. E.W.E. MICKLETHWAITE, "Soil Mechanics in Relation to Fighting Vehicles," Military College of Science, Chertsey, England, 1944.

3. I. EVANS, "The Sinkage of Tracked Vehicles on Soft Ground," J. Terramechanics, Vol. 1, No. 2, 33 (1964).

4. F.L. UFFELMAN, "The Performance of Rigid Cylindrical Wheels on Clay Soil," Proceedings of the First International Conference on Mechanics of Soil-Vehicle Systems, Turin, 1961.

5. M.G. BEKKER, "Off the Road Locomotion," University of Michigan Press, Ann Arbor, 1960.

6. A.D. SELA and I.R. EHRLICH, "Load Support Capability of Flat Plates of Various Shapes in Soils," SAE Paper No. 710178, January 1971.

7. A.D. SELA and I.R. EHRLICH, "Predicting the Performance of Rigid Wheels in Soft Soils at Zero Slip." To be published.

8. E.T. VINCENT, "Pressure Distribution On and Flow of Sand Past a Rigid Wheel," Proceedings of the First International Conference on the Mechanics of Soil Vehicle Systems.

9. E. HEGEDUS, "A Preliminary Analysis of the Force System Acting on a Rigid Wheel," A.S.A.E. Transactions, 1962.

10. A.D. SELA, "The Shear to Normal Stress Relationship between a Rigid Wheel and Dry Sand," Land Locomotion Laboratory Report No. 99, ATAC, Warren, Michigan, 1964.

11. O. ONAFEKO and A.R. REECE, "Soil Stresses and Deformations Beneath Rigid Wheels," J. Terramechanics, Vol. 4, No. 1, 1967.

12. G. KRICK, "Radial and Shear Stress Distribution under Rigid Wheels and Pneumatic Tires Operating on Yielding Soils with Consideration of Tire Deformation," J. Terramechanics, Vol. 6, No. 3, 1969.

13. A.R. REECE, "Principles of Soil Vehicle Mechanics," Proc. Auto. Div. Instn. Mech. Engrs. 180 Pt. 2A, No. 2, 1965-1966.

14. A.D. SELA, "On Slip and Tractive Effort," Proc. First Int. Conf. Mech. Soil-Vehicle Systems, Turin, 1961.

15. Z. Janosi and B. Hanamoto, "The Analytical Determination of Drawbar-Pull as a Function of Slip for Tracked Vehicles in Deformable Soils," Proc. First Int. Conf. Mech. Soil-Vehicle Systems, Turin, 1961.

16. K.W. WEINDIECK, Discussion on "Soil Stresses and Deformations beneath Rigid Wheels," by O. Onafeko and A.R. Reece, J. Terramechanics, Vol. 5, No. 1, 1963.

VITA

Samuel E. Shamaywas born on 14 December 1941 in Cairo, Egypt. He immigrated with his parents to Israel in 1956. He attended high school in Natanya, Israel and graduated from "The Technion" Israel Institute of Technology in 1967 with a Bachelor of Science degree in Mechanical Engineering. The same year he entered the Israeli Army. As a career officer he is now a Lieutenant in the Ordnance Corps.

APPENDIX

This Appendix contains all the raw data gathered during the tests.

Tables I, II and III contain all the results of the tests, except the stress distribution reading.

Tables IV, V and VI contain the data for the stress distribution readings. In these tables, only the data read by the center transducer is listed. For the other three transducers, only the values of the peak stresses are listed because their curves are identical in shape with the first one.

Gauge number 1 is at the center of the wheel, number 4 is close to the edge.

Table 1

RAW DATA TEST LOAD - 200 LBS

Test No.	V_c (ft/sec)	V_w (ft/sec)	Slip (%)	Sinkage (in)	Load (lb)	DP (lb)	Torque (ft-lb)
200-1-1	1.16	1.2	3.3	1.7	200	0	55
200-1-2	1.14	1.17	2.5	1.7	200	0	50
200-2-1	1.0	0.83	-20.5	1.8	195	-50	25
200-2-2	1.0	0.77	-30.0	1.9	200	-60	10
200-2-3	0.93	0.83	-12	1.7	210	-25	30
200-3-1	0.7	0.6	-16.6	1.8	200	-30	30
200-3-2	0.625	0.57	- 9.6	1.7	210	-22	50
200-4-1	0.57	0.545	- 4.6	1.7	200	-1.0	50
200-4-2	0.55	0.5	- 4	1.7	210	-10	50
200-4-3	0.375	0.4	6.3	1.7	205	10	80
200-5-1	0.333	0.33	- 1	1.7	200	- 5	50
200-5-2	0.25	0.255	4	1.7	200	- 2	60
200-6-1	0.277	0.407	32	2.2	200	40	110
200-6-2	0.227	0.366	38.2	2.5	200	40	110
200-6-3	0.152	0.314	52	2.8	200	45	110

Table 2

RAW DATA TEST LOAD - 350 LBS

Test No.	V_c (ft/sec)	V_w (ft/sec)	Slip (%)	Sinkage (in)	Load (lb)	DP (lb)	Torque (ft-lb)
350-1-1	1.11	1.14	2.6	2.7	340	- 4	125
350-1-2	1.11	1.12	0.8	2.7	340	- 5	125
350-1-3	1.00	1.09	8.3	3.0	345	20	135
350-2-1	1.00	0.88	-13.6	2.8	345	-50	50
350-2-2	0.95	0.83	-14.4	2.8	345	-50	50
350-3-1	0.91	0.83	- 9.6	2.7	345	-50	75
350-3-2	0.825	0.74	-11.5	2.7	350	-50	85
350-4-1	0.62	0.63	1.6	2.7	350	- 5	130
350-5-1	0.465	0.515	9.7	3.0	350	20	158
350-6-1	0.345	0.416	17	3.1	350	30	170
350-6-2	0.244	0.284	14.1	3.0	350	25	160
350-6-3	0.140	0.165	15	3.0	350	25	160
350-7-1	0.361	0.672	46.5	4.0	350	35	230
350-7-2	0.274	0.624	56	4.3	350	35	235
350-7-3	0.200	0.588	66	4.7	350	35	235

Table 3

RAW DATA TEST LOAD - 500 LBS

Test No.	V_c (ft/sec)	V_w (ft/sec)	Slip (%)	Sinkage (in)	Load (lb)	DP (lb)	Torque (ft/lb)
500-1-1	1.25	1.14	-9.5	4.2	500	-20	170
500-1-2	1.00	1.02	2	4.2	500	- 5	225
500-1-3	1.00	1.09	8.3	4.3	500	5	230
500-2-1	0.82	1.01	14.0	4.5	500	15	240
500-2-2	0.80	0.95	15.8	4.5	500	15	250
500-3-1	0.79	0.91	13	4.5	500	15	235
500-3-2	0.60	0.65	20	4.7	500	20	280
500-4-1	0.56	0.73	23	4.7	500	25	280
500-4-2	0.50	0.625	25	4.8	500	28	300
500-4-3	0.445	0.635	30	5.0	500	30	300
500-5-1	0.345	0.485	29	5.0	500	30	300
500-5-2	0.25	0.41	39	5.2	500	30	300
500-7-1	0.58	0.65	11	4.4	500	10	265
500-7-2	0.445	0.56	21.5	4.6	500	20	280
500-8-1	0.14	0.22	36.5	5.1	500	30	300

Table 4

STRESS DISTRIBUTION READINGS; 200 LBS

	Test #200-1-1		Test #200-1-2		Test #200-2-1	
α (degrees)	p (psi)	s (psi)	p (psi)	s (psi)	p (psi)	s (psi)
- 5	0.35	0	0.18	0	0	0
0	3.2	1.06	2.66	1.42	2.86	-0.9
5	9.6	2.12	8.9	4.26	9.6	-0.35
10	12.4	1.84	12.1	3.9	12.8	0.35
15	12.8	2.12	12.1	3.9	11.8	1.06
20	11.4	2.32	10.8	4.6	9.6	1.8
25	6.0	1.78	4.6	2.13	6.0	2.14
30	0.71	0	0.35	0	1.8	1.06
35	0	0	0	0	0	0
Gauge No.	Peak Stresses p	s	Peak Stresses p	s	Peak Stresses p	s
1	12.8	2.32	12.1	4.6	12.8	2.14
2	12.4	2.1	11.6	3.6	12.4	2.14
3	12.4	2.1	10:6	2.84	11.0	1.42
4	11.4	1.78	10.3	1.78	10.6	1.06

Table 4 (continued)

Stress Distribution Readings; 200 lbs

α (degrees)	Test #200-2-2 p (psi)	Test #200-2-2 s (psi)	Test #200-2-3 p (psi)	Test #200-2-3 s (psi)	Test #200-3-1 p (psi)	Test #200-3-1 s (psi)
-5	0.35	-0.35	0.35	-0.35	1.06	-1.06
0	4.24	-1.24	3.5	-1.06	6.4	-1.06
5	10.0	-0.71	11.4	-0.53	13.2	-0.71
10	13.0	-0.28	13.2	0.35	13.2	+0.35
15	11.0	+0.53	12.1	0.71	11.8	0.89
20	7.8	1.42	8.2	2.14	8.9	1.42
25	3.5	1.24	3.5	1.42	4.3	2.14
30	0	0	0	0	0.35	0.35
35	0	0	0	0	0	0

Gauge No.	Peak Stresses p	Peak Stresses s	Peak Stresses p	Peak Stresses s	Peak Stresses p	Peak Stresses s
1	13	1.42	13.2	2.14	13.2	2.14
2	12.5	1.25	13.0	2.14	13.0	2.14
3	11.2	0.89	12.1	1.42	12.1	1.8
4	10.8	0.71	11.4	1.06	11.4	1.06

Table 4 (continued)

Stress Distribution Readings; 200 lbs

	Test #200-3-2		Test #200-4-1		Test #200-4-2	
α (degrees)	p (psi)	s (psi)	p (psi)	s (psi)	p (psi)	s (psi)
-5	1.42	-0.71	0	0	0	0
0	8.50	-0.35	2.14	-0.71	2.84	-0.35
5	14.2	+0.35	8.2	-0.35	11.0	1.42
10	13.6	0.71	12.8	0	13.2	1.78
15	12.1	1.06	12.8	0.35	12.8	2.14
20	8.2	1.96	11.8	0.89	11.0	2.5
25	3.5	2.14	8.2	1.78	5.0	1.78
30	0	0	3.2	1.42	0	0
35	0	0	0	0	0	0
	Peak Stresses		Peak Stresses		Peak Stresses	
Gauge No.	p	s	p	s	p	s
1	14.2	2.14	12.8	1.78	13.2	2.5
2	13.8	2.14	12.8	1.78	12.8	2.5
3	13.2	1.78	12.8	1.78	11.8	2.14
4	12.4	1.42	11.8	1.42	11.8	1.78

Table 4(continued)

Stress Distribution Readings; 200 lbs

	Test #200-4-3		Test #200-5-1		Test #200-5-2	
α (degrees)	p (psi)	s (psi)	p (psi)	s (psi)	p (psi)	s (psi)
-5	0	0	0	0	0.35	0
0	3.5	1.42	2.14	-0.2	2.84	0.71
5	10.3	2.5	9.2	1.06	10.3	2.5
10	12.1	2.5	12.1	1.06	12.8	2.5
15	12.1	2.5	12.1	1.42	12.8	2.84
20	10.0	2.84	10.3	1.78	10.3	2.84
25	4.7	1.78	5.0	1.42	1.78	0.71
30	0	0	0	0	0	0
	Peak Stresses		Peak Stresses		Peak Stresses	
Gauge No.	p	s	p	s	p	s
1	12.1	2.84	12.1	1.78	12.8	2.84
2	11.4	2.8	11.7	1.78	12.4	2.84
3	11.4	2.5	11.4	1.42	12.1	2.5
4	11.4	2.5	11.4	1.06	11.7	1.78

Table 4 (continued)

Stress Distribution Readings; 200 lbs.

	Test #200-6-1		Test #200-6-2		Test #200-6-3	
α (degrees)	p (psi)	s (psi)	p (psi)	s (psi)	p (psi)	s (psi)
-5	0.71	0	0.71	0	0.35	0.35
0	1.78	1.42	1.06	1.06	1.06	1.78
5	3.9	3.9	2.5	2.5	3.5	3.5
10	6.4	5.3	3.9	3.9	5.7	4.8
15	8.9	7.8	8.7	7.1	6.4	4.8
20	10.5	8.2	11.7	7.5	7.3	5.3
25	11.7	8.0	12.1	7.9	8.9	6.05
30	11.4	7.4	11.0	6.4	11.7	5.2
35	3.1	2.12	4.6	3.5	2.12	1.06
40	0	0	0	0	0	0
	Peak Stresses		Peak Stresses		Peak Stresses	
Gauge No.	p	s	p	s	p	s
1	11.7	8.2	12.1	7.9	11.7	6.05
2	9.5	6.5	9.6	6.4	9.2	4.8
3	9.0	5.7	9.2	5.7	8.5	3.5
4	8.7	3.5	8.9	3.5	7.6	1.78

Table 5

Stress Distribution Readings; 350 lbs

	Test #350-1-1		Test #350-1-2		Test #350-1-3	
α (degrees)	p (psi)	s (psi)	p (psi)	s (psi)	p (psi)	s (psi)
-10	0	0	0	0	0	0
- 5	0.2	0	0	0	0.9	0.71
0	2.84	0.35	3.2	0.35	3.5	2.5
5	11.4	1.78	13.2	3.2	12.1	3.5
10	14.6	2.14	16.4	3.9	16.4	2.5
15	14.6	2.5	16.7	4.7	16.4	2.5
20	13.2	2.84	16.0	5.0	14.9	3.5
25	8.9	2.84	12.4	5.0	12.1	3.9
30	3.2	1.42	9.2	4.7	5.0	3.2
35	0.71	0.35	1.7	0.71	0.71	0.35
40	0.35	0	0.71	0.35	0	0
45	0	0	0	0	0	0
	Peak Stresses		Peak Stresses		Peak Stresses	
Gauge No.	p	s	p	s	p	s
1	14.6	2.84	16.7	5	16.4	3.9
2	14.6	2.84	15.0	4.7	15.3	3.9
3	14.2	2.5	14.2	3.2	15.3	3.5
4	13.8	1.78	13.8	2.14	14.2	2.5

Table 5 (continued)

Stress Distribution Readings; 350 lbs

	Test #350-2-1		Test #350-2-2		Test #350-3-1	
α (degrees)	p (psi)	s (psi)	p (psi)	s (psi)	p (psi)	s (psi)
-15	0	0	0	0	0	0
-10	0	0	0	0	0	0
- 5	0.71	0	0.35	-0.35	0.35	-0.35
0	3.5	-1.03	3.2	-0.71	4.7	-1.06
5	11.3	-0.35	11.0	-0.35	14.2	1.42
10	15.9	+0.35	16.0	+0.35	16.4	1.42
15	15.6	1.78	15.2	0.71	16.4	2.14
20	13.8	2.84	14.2	1.42	14.9	2.84
25	9.9	3.9	11.0	1.78	11.4	3.2
30	5.3	3.2	5.0	1.78	5.7	2.84
35	0.71	0.71	0.35	0.35	0.71	0.35
40	0	0	0	0	0	0
45	0	0	0	0	0	0
	Peak Stresses		Peak Stresses		Peak Stresses	
Gauge No.	p	s	p	s	p	s
1	15.9	3.9	16.0	1.78	16.4	3.2
2	15.6	3.2	14.9	1.78	15.2	2.84
3	15.2	2.84	14.9	1.42	15.2	2.5
4	14.8	2.5	14.2	1.06	14.2	1.42

Table 5 (continued)

Stress Distribution Readings; 350 lbs

	Test #350-3-2		Test #350-4-1		Test #350-5-1	
α (degrees)	p (psi)	s (psi)	p (psi)	s (psi)	p (psi)	s (psi)
-15	0	0	0	0	0	0
-10	0	0	0	0	0	0
- 5	1.06	-0.71	1.78	0.71	0	0
0	6.4	-1.06	9.6	2.6	3.5	0.71
5	15.7	-0.71	14.9	2.1	12.8	2.14
10	16.8	0	16.0	2.1	16.4	2.84
15	15.3	+0.35	15.6	2.84	17.0	2.84
20	14.2	0.71	14.2	2.84	15.6	3.5
25	10.6	1.78	11.4	2.84	12.8	3.5
30	5.0	2.14	5.3	2.1	7.8	3.5
35	1.06	1.06	0	0	2.14	1.42
40	0	0	0	0	0	0
45	0	0	0	0	0	0
	Peak Stresses		Peak Stresses		Peak Stresses	
Gauge No.	p	s	p	s	p	s
1	16.8	2.14	16.0	2.84	17.0	3.5
2	15.7	1.78	15.7	2.84	17.0	3.5
3	15.7	1.78	15.0	2.14	15.6	3.5
4	14.2	1.42	14.2	1.78	15.6	2.14

Table 5 (continued)

Stress Distribution Readings; 350 lbs

α (degrees)	Test #350-6-1 p (psi)	Test #350-6-1 s (psi)	Test #350-6-2 p (psi)	Test #350-6-2 s (psi)	Test #350-6-3 p (psi)	Test #350-6-3 s (psi)
-15	0	0	0	0	0	0
-10	2	1	0	0	0	0
- 5	3.42	1.42	0.71	0.71	1.42	1.42
0	7.4	4.2	9.2	6.0	8.5	5
5	13.0	5.0	14.2	5.7	14.2	5
10	16.2	5.0	17.0	5.7	16.5	4.2
15	14.5	5.7	17.0	5.7	15.7	5
20	13.8	5.7	14.2	6.0	14.3	5.7
25	10.6	5.0	10.6	6.0	12.2	5.7
30	4.2	2.14	5.0	3.5	5.7	3.5
35	2	0	2.8	0.71	0	0
40	0	0	0	0	0	0
45	0	0	0	0	0	0
	Peak Stresses		Peak Stresses		Peak Stresses	
Gauge No.	p	s	p	s	p	s
1	16.2	5.7	17.0	6.0	16.5	5.7
2	13.8	5.0	17.0	5.7	15.7	5.7
3	13.0	5.0	16.3	5.0	15.0	5.0
4	12.0	2.84	15.6	3.5	15.0	4.2

Table 5 (continued)

Stress Distribution Readings; 350 lbs

	Test #350-7-1		Test #350-7-2		Test #350-7-3	
α (degrees)	p (psi)	s (psi)	p (psi)	s (psi)	p (psi)	s (psi)
-15	0	0	0	0	0	0
-10	1.42	1.42	0.71	0.71	1.42	1.42
- 5	4.25	3.5	1.42	1.42	2.14	2.14
0	5.32	5.0	3.5	3.5	2.84	2.84
5	7.1	5.7	8.4	7.8	5.0	5.0
10	11.8	7.6	11.4	7.8	9.1	5.7
15	14.8	7.6	11.4	7.8	10.7	7.1
20	15.7	8.2	14.9	7.1	13.5	6.4
25	15.0	8.2	16.3	7.1	16.0	5.0
30	14.3	8.0	13.5	6.4	14.2	3.5
35	8.6	5	6.4	4.3	12.1	2.84
40	2.3	1.42	4.3	2.14	3.5	2.14
45	0	0	0	0	0	0
	Peak Stresses		Peak Stresses		Peak Stresses	
Gauge No.	p	s	p	s	p	s
1	15.5	8.2	16.3	7.8	17.0	7.1
2	14.2	8.2	14.2	7.1	14.2	6.4
3	12.8	7.1	12.1	6.4	11.4	5.7
4	10.6	5.7	10.6	2.14	8.4	5.0

Table 6

Stress Distribution Readings; 500 lbs

	Test #500-1-1		Test #500-1-2		Test #500-1-3	
α (degrees)	p (psi)	s (psi)	p (psi)	s (psi)	p (psi)	s (psi)
-15	0	0	0	0	0	0
-10	0	0	0	0	0	0
- 5	3.5	-0.71	0.71	0.71	1.42	1.42
0	12.8	-1.42	10.0	3.5	9.2	2.84
5	22.0	-2.3	17.0	2.8	15.6	3.55
10	24.8	-1.42	23.4	2.3	22.7	2.14
15	23.4	0	25.5	2.3	25.5	1.42
20	20.0	+1.42	23.4	3.5	22.7	2.84
25	16.3	+2.3	18.4	4.2	18.4	3.55
30	10.8	+2.84	14.2	5.0	12.0	4.25
35	7.1	+2.3	8.6	4.7	5.7	3.55
40	2.3	+1.42	2.3	0.71	1.42	1.42
45	0	0	0	0	0	0
	Peak Stresses		Peak Stresses		Peak Stresses	
Gauge No.	p	s	p	s	p	s
1	24.8	2.84	25.5	5.0	25.5	4.25
2	24.1	2.14	24.8	4.25	24.8	3.55
3	24.1	2.14	24.0	3.55	24.1	2.84
4	23.4	1.42	24.0	2.84	23.4	2.84

Table 6 (continued)

Stress Distribution Readings; 500 lbs

	Test #500-2-1		Test #500-2-2		Test #500-3-1	
α (degrees)	p (psi)	s (psi)	p (psi)	s (psi)	p (psi)	s (psi)
-15	0	0	0	0	0	0
-10	0.35	0	0	0	0.35	0
- 5	2.14	1.42	0.71	0.71	2.14	2.14
0	5.0	3.55	5.0	5.0	6.4	5.0
5	12.7	4.25	11.4	7.1	12.8	5.7
10	17.0	3.55	18.4	5.7	18.4	5.0
15	23.4	2.14	24.8	5.0	24.2	4.3
20	24.8	3.55	25.5	5.0	22.7	4.3
25	22.0	4.28	24.2	5.7	21.4	5.0
30	16.3	4.28	19.2	6.4	17.7	5.7
35	10.6	4.28	12.0	6.4	12.1	5.0
40	4.25	2.14	5	2.14	5.7	2.14
45	0	0	0	0	0	0
	Peak Stresses		Peak Stresses		Peak Stresses	
Gauge No.	p	s	p	s	p	s
1	24.8	4.25	25.5	7.1	24.2	5.7
2	24.2	4.25	24.8	6.4	24.2	5.0
3	24.2	3.55	24.0	6.4	23.4	5.0
4	23.4	2.84	22.7	5.0	22.7	4.3

Table 6 (continued)

Stress Distribution Readings; 500 lbs

	Test #500-3-2		Test #500-4-1		Test #500-4-2	
α (degrees)	p (psi)	s (psi)	p (psi)	s (psi)	p (psi)	s (psi)
-15	0	0	0	0	0	0
-10	0.71	0.71	0.71	0.71	0.71	0.71
- 5	2.14	2.14	2.14	2.14	2.14	2.14
0	5.0	5.0	6.4	5.0	6.4	5.0
5	10.6	5.7	12.8	6.4	12.1	7.1
10	17.7	4.3	17.0	5.7	21.4	7.1
15	22.7	2.84	22.7	5.0	22.7	6.4
20	24.8	2.84	24.8	5.0	25.5	6.4
25	24.1	2.84	23.4	5.7	23.4	7.1
30	20.6	3.55	21.4	6.4	21.4	7.8
35	16.3	4.3	17.0	6.4	13.5	5.0
40	8.5	2.84	10.0	4.3	7.1	3.5
45	2.14	1.42	3.5	2.84	2.14	2.1
50	0	0	0	0	0	0
	Peak Stresses		Peak Stresses		Peak Stresses	
Gauge No.	p	s	p	s	p	s
1	24.8	5.7	24.8	6.4	25.5	7.8
2	24.8	5.7	24.1	5.7	24.2	6.4
3	22.7	5.0	23.4	5.0	21.4	5.7
4	22.0	4.3	22.7	4.3	20.0	4.3

Table 6 (continued)

Stress Distribution Readings; 500 lbs

	Test #500-4-3		Test #500-5-1		Test #500-5-2	
α (degrees)	p (psi)	s (psi)	p (psi)	s (psi)	p (psi)	s (psi)
-15	0	0	0	0	0	0
-10	0.35	0.35	0	0	0.71	0.71
- 5	1.42	1.42	1.42	1.42	1.06	1.06
0	5.7	4.3	3.5	3.5	3.5	3.5
5	12.8	5.7	8.5	6.4	7.8	6.4
10	19.2	4.3	14.9	6.4	14.2	8.6
15	23.4	3.5	20.0	5.0	21.8	7.1
20	25.5	3.5	24.2	4.3	24.2	5.7
25	24.2	3.5	24.9	5.0	25.0	5.7
30	23.4	3.5	22.0	5.7	18.4	7.1
35	12.1	5.0	17.8	6.4	14.2	7.1
40	5.0	5.0	9.2	3.5	10.6	5.7
45	0	0	3.5	2.15	3.5	2.84
50	0	0	0	0	0	0
	Peak Stresses		Peak Stresses		Peak Stresses	
Gauge No.	p	s	p	s	p	s
1	25.5	5.7	24.9	6.4	25	8.6
2	24.2	5.7	24.2	6.4	24.2	7.1
3	21.4	4.3	23.4	5.7	23.4	6.4
4	20.0	3.5	20.0	4.3	20.0	5.0

Table 6 (continued)

Stress Distribution Readings; 500 lbs

	Test #500-7-7		Test #500-7-2		Test #500-8-1	
α (degrees)	p (psi)	s (psi)	p (psi)	s (psi)	p (psi)	s (psi)
-15	0	0	0	0	0	0
-10	0.35	0	0.35	0	0.71	0.71
- 5	1.42	0.71	1.06	0.71	2.14	2.14
0	7.1	3.2	5.3	3.2	3.5	3.5
5	14.5	2.8	12.0	5.0	10.0	7.1
10	23.0	0.71	19.2	3.5	17.1	7.1
15	25.5	0.42	24.2	2.8	24.2	5.7
20	24.2	1.42	24.9	3.5	25.5	5.7
25	20.0	2.35	20.6	4.3	24.8	5.7
30	14.0	2.84	15.6	3.2	22.7	5.7
35	7.1	2.84	10.0	2.8	10.0	5.7
40	3.5	1.4	4.27	1.42	5.7	2.8
45	0	0	0	0	1.42	1.42
	Peak Stresses		Peak Stresses		Peak Stresses	
Gauge No.	p	s	p	s	p	s
1	25.5	2.84	24.9	5.0	25.5	7.1
2	24.8	2.84	24.1	4.3	24.8	6.4
3	24.0	2.14	22.7	4.3	24.2	6.4
4	22.7	1.78	22.0	3.5	23.4	5.7